Phys. Lett. B 856 (2024) 138925

Contents lists available at ScienceDirect

Physics Letters B

journal homepage: www.elsevier.com/locate/physletb

Letter

Primordial non-Gaussianity as a saviour for PBH overproduction in SIGWs generated by pulsar timing arrays for Galileon inflation

Sayantan Choudhury [a,*], Kritartha Dey [a], Ahaskar Karde [a], Sudhakar Panda [a,b], M. Sami [a,c,d]

[a] Centre For Cosmology and Science Popularization (CCSP), SGT University, Gurugram, Delhi - NCR, Haryana - 122505, India
[b] School of Physical Sciences, National Institute of Science Education and Research, Bhubaneswar, Odisha - 752050, India
[c] Center for Theoretical Physics, Eurasian National University, Astana 010008, Kazakhstan
[d] Chinese Academy of Sciences, 52 Sanlihe Rd, Xicheng District, Beijing, China

ARTICLE INFO

Editor: M. Trodden

ABSTRACT

We investigate the explicit role of negative local non-Gaussianity, $f_{\rm NL}$, in suppressing the abundance of primordial black holes (PBHs) in the single-field model of Galileon inflation. PBH formation requires significantly enhancing the scalar power spectrum, which greatly affects their abundance. The associated frequencies in the nHz regime are also sensitive to the generation of scalar-induced gravitational waves (SIGWs) which may explain the current data from the pulsar timing arrays (PTAs). Our analysis using the threshold statistics on the compaction function demonstrates that Galileon theory not only avoids PBH overproduction using the curvature perturbation enhancements that give $f_{\rm NL} \sim \mathcal{O}(-6)$, but also generates SIGWs that conform well with the PTA data.

Recent findings from the pulsar timing array (PTA) collaborations, which include the NANOGrav [1–8], EPTA [9–14], PPTA [15–17], and CPTA [18], have confirmed the observed common-spectrum signal for a stochastic gravitational wave background (SGWB). Since then, considerable works have discussed the interpretations and possible cosmological origins of the signal, such as first-order phase transitions, cosmic strings, domain walls, and inflation, particularly scalar-induced gravitational waves (SIGWs). (See refs. [19–78]). Such cosmological scenarios contain models that better agree with the PTA data. However, this letter focuses on the SIGW interpretation of the PTA signal and concerns related to the primordial black hole (PBH) production associated with the frequency regime of the signal.

Scalar-induced GWs manifest as the tensor perturbations at second-order induced by curvature perturbations in the spatially flat FLRW background upon horizon re-entry. [79–83]. At the same time, during inflation, small-scale enhancements in the curvature perturbations lead to the generation of overdense and underdense regions in the density contrast field, which, on exceeding a threshold overdensity, gravitationally collapses to form PBHs [83–204]. However, in some cases, PBHs may also get overproduced [22,27,28,205,206]. The general mechanism for PBH production in single-field inflationary models necessitates an ultra-slow roll (USR) phase, which sufficiently amplifies the scalar power spectrum amplitude [19,195,204,207–221]. This USR phase raises concerns about generating large non-Gaussianities (NGs) [213], challenging the Gaussian statistics assumption for the comoving curvature perturbations. Accurately assessing the PBH abundance, as the fraction constituting all of present-day dark matter, requires a careful account of the primordial NGs. Recent attempts to tackle PBH overproduction involve strategies like incorporating an extra spectator field along with the metric perturbations, as in the curvaton model [22,222,223] or an additional spectator tensor field [27], while positive NG is declared harmful to the PBH abundance, especially in non-attractor single-field models [224]. The total PBH abundance heavily depends on the NG magnitude and its signature. Requiring a sizeable abundance largely impacts the peak of the scalar power spectrum, thereby putting constraints on the maximum of the observed SIGW spectrum.

In this letter, we aim to demonstrate that PBH overproduction does not occur in the non-attractor single-field inflation model described by covariantized Galileon theory, which includes a USR phase while accounting for the primordial NGs and intrinsic non-linearities between the density fluctuations and the comoving curvature perturbations.

* Corresponding author.
E-mail addresses: sayantan_ccsp@sgtuniversity.org, sayanphysicsisi@gmail.com (S. Choudhury), kritartha09@gmail.com (K. Dey), kardeahaskar@gmail.com (A. Karde), panda@niser.ac.in (S. Panda), sami_ccsp@sgtuniversity.org, samijamia@gmail.com (M. Sami).

https://doi.org/10.1016/j.physletb.2024.138925
Received 30 October 2023; Received in revised form 26 July 2024; Accepted 28 July 2024
Available online 31 July 2024

The study by authors in ref. [213] demonstrates significant negative NG, $f_{\rm NL} \sim \mathcal{O}(-6)$, generated in the USR phase of Galileon theory. Its unique non-renormalization theorem strongly suggests suppression of the quantum loop corrections within the theory, allowing no constraints on the allowed PBH masses [19,212,213]. This property also provides us with the advantage of allowing for successful inflation. Our findings from Galileon reveal that large negative NGs allow for a sizeable abundance of PBH and a substantial scalar power spectrum amplitude, consistent with the recent NANOGrav 15 data. Another reason, observationally speaking, for working with Galileon comes from the results in [19], where the SIGW spectrum generated shows consistency with the NANOGrav 15 signal and, thanks to the intrinsic features of this theory, it also shows signatures in the parameter space of the existing and future GW experiments, including LISA [225], DECIGO [226], ET [227], CE [228], BBO [229], HLVK [230–232], and HLV(O3) [230–232].

We employ the approach of threshold statistics on the compaction function parameter to accurately investigate the PBH abundance [22,205,233–238]. This procedure helps us to picture the non-linear corrections to the density contrast and include the primordial NGs in the curvature perturbation within the framework of covariantized Galileon theory.

We start by briefly laying out the underlying features of the Galileon inflation theory [239] used in this paper. A remarkable quality of this theory is that despite the action containing a higher-derivative structure one obtains equations of motion quadratic in the scalar field ϕ which is known here as the Galileon field. The theory comes equipped with a unique symmetry known as the Galilean shift symmetry, which in a $3+1$ spacetime can be written as follows:

$$\phi \to \phi + v_\mu x^\mu + b, \tag{1}$$

where b is a constant scalar, v^μ is a constant vector, x^μ represent the spacetime variable. We will return to the use of this symmetry when we talk about the importance of the non-renormalization theorem and quantum loop effects in Galileon theory. We mostly focus on the dynamics of this Galileon field in a inflationary scenario where the background spacetime has a quasi de-Sitter geometry, such that the effective potential during inflation satisfies the condition $|\Delta V/V| \ll 1$ and the expansion is characterized by the necessary slow-roll conditions. The action for the Galileon field in the background, $\bar{\phi}(t)$ reads:

$$S^{(0)} = \int d^4x\, a^3 \left[\dot{\bar{\phi}}^2 \left\{ \frac{c_2}{2} + 2c_3 Z + \frac{9c_4}{2} Z^2 + 6c_5 Z^3 \right\} + c_1 \bar{\phi} \right], \quad \text{where} \quad Z \equiv H\dot{\bar{\phi}}/\Lambda^3, \quad c_1 = \lambda^3, \tag{2}$$

with $c_i \forall\, i = 1, \cdots, 5$ representing the coefficients that parameterize the Galileon theory, λ is a mass dimension 1 parameter that also helps to characterize the exact shift symmetry breaking in the potential, and the action involves the coupling parameter, Z, in terms of the physical cut-off scale, Λ, of the theory. From here the task of computing the scalar power spectrum involves expanding this action to second order in the perturbations around the background, more details on this construction and the comoving curvature perturbation can be found in ref. [212]. This perturbed second-order action in the Fourier space reads as follows:

$$S^{(2)}_\zeta = \int d\tau\, \frac{d^3\mathbf{k}}{(2\pi)^3} a^2(\tau) \frac{\mathcal{A}}{H^2} \left(|\zeta'_{\mathbf{k}}(\tau)|^2 - c_s^2 k^2 |\zeta_{\mathbf{k}}(\tau)|^2 \right), \quad \text{where} \quad c_s^2 = \frac{\mathcal{B}}{\mathcal{A}}, \tag{3}$$

here $\zeta_{\mathbf{k}}(\tau)$ is the Fourier space comoving curvature perturbation mode function, $a(\tau) = -1/H\tau$ is the scale factor in conformal time coordinates and, $\mathcal{A}, \mathcal{B}$, are the time-dependent coefficients having relation with c_s as the effective sound speed parameter of our theory. These coefficients have the following specific expressions:

$$\mathcal{A} \equiv \frac{\dot{\bar{\phi}}^2}{2} \left(c_2 + 12c_3 Z + 54c_4 Z^2 + 120c_5 Z^3 \right), \tag{4}$$

$$\mathcal{B} \equiv \frac{\dot{\bar{\phi}}^2}{2} \left\{ c_2 + 4c_3 \left(2Z - \frac{H\dot{\bar{\phi}}}{\Lambda^3}\eta \right) + 2c_4 \left[13Z^2 - \frac{6}{\Lambda^6} \times \dot{\bar{\phi}}^2 H^2 (\epsilon + 2\eta) \right] - \frac{24c_5}{\Lambda^9} H^3 \dot{\bar{\phi}}^3 (2\epsilon + 1) \right\}, \tag{5}$$

and they also include the first and second slow-roll parameters, $\epsilon = -\dot{H}/H^2$ and $\eta = \dot{\epsilon}/\epsilon H$, respectively. Important to note is the fact that the values of the dimensionless coefficients, $\{c_i\ \forall i = 1 \text{ to } 5\}$, and the coupling Z and field $\bar{\phi}(t)$, are chosen in such a manner to allow for the parameter c_s taking proper values that satisfy causality and unitarity constraints during inflation. Also, the chosen values help to set up an additional ultra-slow roll phase for the brief duration of $\Delta\mathcal{N}_{\rm USR} \sim \mathcal{O}(2)$ in the present theory [240]. We hereafter aim to consider the scalar power spectrum from Galileon theory, accounting for the quantum one-loop corrections originating due to the perturbed action at cubic order. The complete construction of such an action and dealing with the quantum loop effects requires understanding the significance of the non-renormalization theorem to which we now allude.

The non-renormalization theorem provides a great deal of simplicity in the computation of one-loop effects in Galileon theory as it allows us to completely do away with operators that bring significant radiative corrections to its Lagrangian. Since we focus on an inflationary scenario from the start, a mild shift symmetry breaking is needed to realise the same physically. However, under such a soft symmetry-breaking condition, the non-renormalization theorem remains valid since the Galileon theory operators, along with any couplings of the heavy fields to the Galileon, respect the Galilean shift symmetry. This feature protects the Lagrangian against any harmful renormalizations that destroy its stability [239,241]. Consider the Galilean symmetry in eqn. (1). Under this symmetry the comoving curvature perturbation transform in the following manner:

$$\zeta \to \zeta - \frac{H}{\dot{\bar{\phi}}} v.\delta x \tag{6}$$

from which we can deduce that the terms ζ, ζ', and $\partial_i\zeta$, all break Galilean shift symmetry mildly, and only $\partial^2\zeta$ remains invariant due to its double derivative structure. Using the above transformation properties one can construct operators as a combination of these terms that exhibit the mild symmetry breaking needed for inflation. After going through the algebra of removing any redundant contributions via field re-definitions and other boundary terms, we remain with only a few acceptable terms such as, ζ'^3, $\zeta'^2\partial^2\zeta$, $\zeta'(\partial_i\zeta)^2$ and $(\partial_i\zeta)^2\partial^2\zeta$, which later form the cubic order action. We now provide a glimpse of this said cubic action that is responsible for the quantum loop effects calculations:

$$S^3_\zeta = \int d\tau\, d^3x \frac{a(\tau)^2}{H^3} \left[\frac{\mathcal{G}_1}{a}\zeta'^3 + \frac{\mathcal{G}_2}{a^2}\zeta'^2 (\partial^2\zeta) + \frac{\mathcal{G}_3}{a}\zeta' (\partial_i\zeta)^2 + \frac{\mathcal{G}_4}{a^2} (\partial_i\zeta)^2 (\partial^2\zeta) \right]. \tag{7}$$

We do not list here explicitly the Galileon operators coefficients, $\mathcal{G}_i\ \forall i = 1, \cdots, 4$, due to their complex structure and would be irrelevant, but their exact expressions can be found in [212]. The actual one-loop computation requires following the Schwinger-Keldysh (*in-in*) formalism, and its implementation results in the two-point correlation function read as follows:

$$\langle \hat{\zeta}_{\mathbf{k}} \hat{\zeta}_{-\mathbf{k}} \rangle = \lim_{\tau\to 0} \left\langle \left[\overline{T} \exp\left(i \int_{-\infty(1-i\epsilon)}^{\tau} d\tau'\, H_{\rm int}(\tau') \right) \right] \hat{\zeta}_{\mathbf{k}}(\tau) \hat{\zeta}_{-\mathbf{k}}(\tau) \left[T \exp\left(-i \int_{-\infty(1+i\epsilon)}^{\tau} d\tau''\, H_{\rm int}(\tau'') \right) \right] \right\rangle, \tag{8}$$

where inside the above expression, we expand the interaction Hamiltonian and upto leading order obtain the relevant one-loop contributions after plugging inside, $H_{\rm int} = -\mathcal{L}^3$, using the action in eqn. (7). This identification of $H_{\rm int}$ works specifically at the third order. All that now remains is to calculate the following in-in correlations:

$$\langle\hat{\zeta}_{\mathbf{k}}\hat{\zeta}_{-\mathbf{k}}\rangle_{(0,0)} = \langle\hat{\zeta}_{\mathbf{k}}\hat{\zeta}_{-\mathbf{k}}\rangle_{\mathbf{Tree}} = \lim_{\tau\to 0}\langle\hat{\zeta}_{\mathbf{k}}(\tau)\hat{\zeta}_{-\mathbf{k}}(\tau)\rangle, \tag{9}$$

$$\langle\hat{\zeta}_{\mathbf{k}}\hat{\zeta}_{-\mathbf{k}}\rangle_{(0,2)} = \lim_{\tau\to 0}\int_{-\infty}^{\tau} d\tau_1 \int_{-\infty}^{\tau} d\tau_2\, \langle\hat{\zeta}_{\mathbf{k}}(\tau)\hat{\zeta}_{-\mathbf{k}}(\tau)H_{\rm int}(\tau_1)H_{\rm int}(\tau_2)\rangle, \tag{10}$$

$$\langle\hat{\zeta}_{\mathbf{k}}\hat{\zeta}_{-\mathbf{k}}\rangle^{\dagger}_{(0,2)} = \lim_{\tau\to 0}\int_{-\infty}^{\tau} d\tau_1 \int_{-\infty}^{\tau} d\tau_2\, \langle\hat{\zeta}_{\mathbf{k}}(\tau)\hat{\zeta}_{-\mathbf{k}}(\tau)H_{\rm int}(\tau_1)H_{\rm int}(\tau_2)\rangle^{\dagger}, \tag{11}$$

$$\langle\hat{\zeta}_{\mathbf{k}}\hat{\zeta}_{-\mathbf{k}}\rangle_{(1,1)} = \lim_{\tau\to 0}\int_{-\infty}^{\tau} d\tau_1 \int_{-\infty}^{\tau} d\tau_2\, \langle H_{\rm int}(\tau_1)\hat{\zeta}_{\mathbf{k}}(\tau)\hat{\zeta}_{-\mathbf{k}}(\tau)H_{\rm int}(\tau_2)\rangle, \tag{12}$$

$$\langle\hat{\zeta}_{\mathbf{k}}\hat{\zeta}_{-\mathbf{k}}\rangle_{\mathbf{One-loop}} = \langle\hat{\zeta}_{\mathbf{k}}\hat{\zeta}_{-\mathbf{k}}\rangle_{(0,2)} + \langle\hat{\zeta}_{\mathbf{k}}\hat{\zeta}_{-\mathbf{k}}\rangle^{\dagger}_{(0,2)} + \langle\hat{\zeta}_{\mathbf{k}}\hat{\zeta}_{-\mathbf{k}}\rangle_{(1,1)}. \tag{13}$$

The correlation in eqn. (9) provides the tree-level contribution to the primordial scalar power spectrum while the sum of the correlations in eqns. (10)-(12) provide the necessary one-loop corrections written in eqn. (13). The final power spectrum expression combines the contributions coming from each of the four operators inside eqn. (7) and thus leads to the result as:

$$\langle\hat{\zeta}_{\mathbf{k}}\hat{\zeta}_{-\mathbf{k}}\rangle = \langle\hat{\zeta}_{\mathbf{k}}\hat{\zeta}_{-\mathbf{k}}\rangle_{\mathbf{Tree}} + \langle\hat{\zeta}_{\mathbf{k}}\hat{\zeta}_{-\mathbf{k}}\rangle_{\mathbf{One-loop}}, \tag{14}$$

where the one-loop effects remain highly suppressed when calculated as described above due to the non-renormalization theorem. We however provide the necessary details as it will be helpful to visualize the total power spectrum structure in the upcoming discussions.

The power spectrum associated with the scalar modes is crucial to analyze the SIGW spectrum. Also, the enhancements in the scalar power spectrum of our theory due to the presence of the USR phase will give rise to a peak amplitude corresponding to the maximum abundance of PBHs. We begin by presenting the final cut-off regularized one-loop corrected power spectrum for the scalar modes as follows:

$$\begin{aligned}\Delta^2_{\zeta}(k) = A\left[1+\left(\frac{k}{k_s}\right)^2\right] &\times\left\{\left(\frac{k_s}{k_e}\right)^6\left(1+\mathcal{Q}_c\right) + \left(\left|\alpha^{(2)}_{\mathbf{k}} - \beta^{(2)}_{\mathbf{k}}\right|^2\Theta(k-k_s)\right.\right.\\ &\left.\left.+\left|\alpha^{(3)}_{\mathbf{k}} - \beta^{(3)}_{\mathbf{k}}\right|^2\Theta(k-k_e)\right)\right\},\end{aligned} \tag{15}$$

where $\mathcal{Q}_c$ denotes the one-loop corrections present in the final scalar power spectrum, which becomes suppressed on account of the non-renormalization theorem in the Galileon theory. We refer the readers to [212] for the explicit computations of the loop effects contributions $\mathcal{Q}_c$ resulting from the use of eqns. (10)-(12). Also $k_s/k_e \sim \mathcal{O}(0.1) < 1$. The quantity A represents the amplitude of the scalar power spectrum at the scale k_s, and $\{k_s,\ k_e\}$ denote the transition scales from the first slow-roll (SRI) to the USR and from the USR to the second slow-roll (SRII) phases, respectively. The amplitude A involves the coefficients defined in eqns. (4), (5) and the effective sound speed c_s from eqn. (2). For details regarding the comoving curvature perturbation mode solutions and the scalar power spectrum with Bogoliubov coefficients $\alpha^{(2)}_{\mathbf{k}}$, $\beta^{(2)}_{\mathbf{k}}$, $\alpha^{(3)}_{\mathbf{k}}$, $\beta^{(3)}_{\mathbf{k}}$, see the appendix A. The transition scale, k_s, governs the type of PBH produced within the range of sub-solar to massive solar mass.

The fractional energy density in the currently observed GW spectrum is measured using the total scalar power spectrum from the relation [242]:

$$\Omega_{\rm GW}(f) = 0.39\times\left[\frac{g_*(T_{\rm rad})}{106.75}\right]^{-1/3}\Omega_{r,0}\times\int_0^{\infty} dy \int_{|1-y|}^{1+y} dx\, \mathcal{G}(x,y)\Delta^2_{\zeta}(kx)\Delta^2_{\zeta}(ky), \tag{16}$$

where the present radiation energy density fraction is denoted by $\Omega_{r,0}$, and $g_*(T_{\rm rad})$ is the relativistic d.o.f. during radiation-dominated (RD) era at the specific temperature $T_{\rm rad}$. The integration kernel is used as:

$$\begin{aligned}\mathcal{G}(x,y) = &\frac{3\left(4x^2-(1+y^2-x^2)^2\right)^2\left(x^2+y^2-3\right)^4}{1024\,x^8y^8}\\ &\times\left[\left(\ln\frac{|3-(x+y)^2|}{|3-(x-y)^2|} - \frac{4xy}{x^2+y^2-3}\right)^2\right.\\ &\left.+\pi^2\Theta(x+y-\sqrt{3})\right].\end{aligned} \tag{17}$$

The relation to convert between the frequency and the wavenumber is used here as:

$$f = 1.6\times 10^{-9}\ {\rm Hz}\left(\frac{k}{10^6{\rm Mpc}^{-1}}\right). \tag{18}$$

The eqn. (16) contains the predominant contribution to the GW spectrum coming from the RD era and behaviour of the peak amplitude of the scalar power spectrum, $\mathcal{O}(10^{-2})$, where the impact of the corrections due to NGs to the curvature perturbation is subdominant. Our task would be to use the total scalar power spectrum as in eqn. (15) to determine the SIGW spectrum within the frequency range sensitive to the NANOGrav 15, as well as the EPTA signal, where we would also examine the production of the PBHs.

Fig. 1 presents our results for the SIGW spectra from Galileon theory superimposed over the NANOGrav 15 and EPTA signal. We plot the spectra for a set of effective sound speed values, $c_s \in \{0.04, 0.05, 0.06\}$, where the condition $f_{\rm NL} \sim \mathcal{O}(-6)$ is satisfied, as shown in [213]. The generated spectra from Galileon theory lie within the observed peak and low-frequency regime of the signals. For the full range of both the signals, the actual trend is obeyed largely by the resulting spectra, which achieves a peak value during the interval of the USR phase where $f \sim \mathcal{O}(10^{-8} - 10^{-7})$Hz.

We now address the central issue concerning the PBH abundance and related significant overproduction issues. An accurate estimation of the abundance requires properly considering the non-linearities between the perturbations in the density contrast field and the comoving curvature given by [236]:

$$\delta(r,t) = -\frac{2}{3}\frac{u}{(aH)^2}e^{-2\zeta(r)}\left[\zeta''(r) + \frac{2}{r}\zeta'(r) + \frac{1}{2}\zeta'(r)^2\right], \tag{19}$$

where $u = 3(1+w)/(5+3w)$ is related to the equation of state parameter w [243]. We will further use $w = 1/3$ for the RD era in the rest of computation. The above equation assumes spherical symmetry for the locally perturbed region and the long wavelength approximation on super-horizon scales. The further inclusion of primordial NGs in the conserved curvature perturbation random field $\zeta(r)$ will then translate into the density contrast field through the above-mentioned non-linear relation. We focus on the quadratic NG model in this work, given by the well-known ansatz:

$$\zeta = \zeta_G + \frac{3}{5}f_{\rm NL}\zeta_G^2, \tag{20}$$

where $\zeta_G \equiv \zeta_G(r)$ follows Gaussian statistics and $f_{\rm NL}$ measures the amount of NG in the theory. We now invoke the threshold statistics approach on the compaction function to accurately estimate PBH abundance in the presence of the above-mentioned features. Details concerning the compaction function can be found in the SM. From the use of eqn. (19), the definition of the compaction function $\mathcal{C}(r,t)$ then acquires a time-independent behaviour valid in the super-horizon scales, resulting in the following expression:

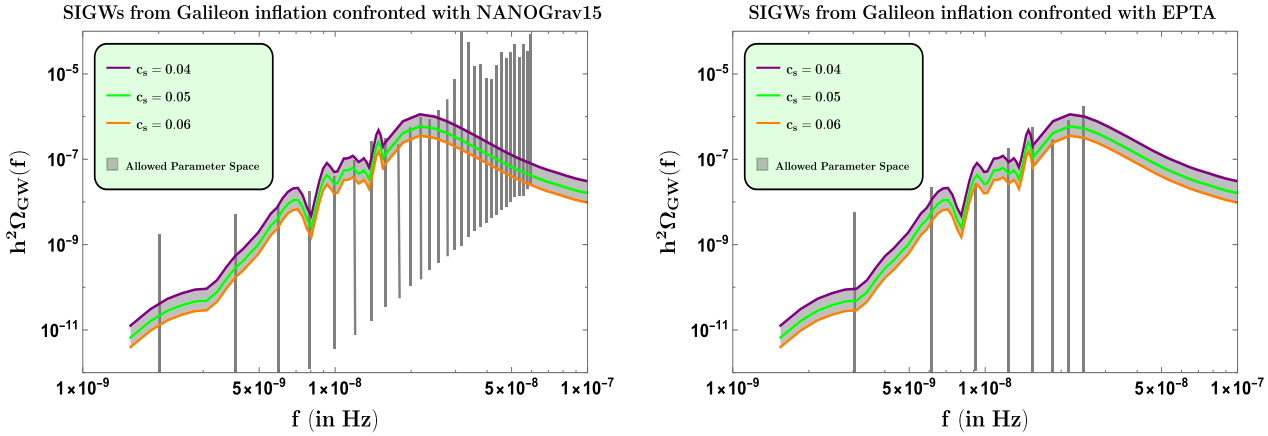

Fig. 1. The SIGW spectra from Galileon theory confronted with the NANOGrav 15 signal (*left-panel*), and with the EPTA signal (*right-panel*). The gray-coloured band illustrates the permissible parameter space for various values of the effective sound speed at the pivot scale, $c_s \in \{0.04, 0.05, 0.06\}$, ensuring $f_{\rm NL} \sim \mathcal{O}(-6)$. The gray lines in the background show the NANOGrav 15 and EPTA signal.

$$C(r) = C_G(r)\frac{d\zeta}{d\zeta_G} - \frac{1}{4u}\left(C_G(r)\frac{d\zeta}{d\zeta_G}\right)^2, \tag{21}$$

where $C_G(r) = -2ur\zeta_G'(r)$. The above relation contains two Gaussian variables: $\zeta_G(r)$ and $C_G(r)$, defined as the derivative of a Gaussian variable. Now, the total fraction of the dark matter present in PBHs comes from after integrating over a range of horizon masses (M_H) in the relation [22,205]:

$$f_{\rm PBH} = \frac{1}{\Omega_{\rm DM}}\int d\,\ln M_H \left(\frac{M_H}{M_\odot}\right)^{-\frac{1}{2}} \times \left(\frac{g_*}{106.75}\right)^{\frac{3}{4}}\left(\frac{g_{*s}}{106.75}\right)^{-1}\left(\frac{\beta_{\rm NG}(M_H)}{7.9\times10^{-10}}\right), \tag{22}$$

where $\Omega_{\rm DM} \simeq 0.264$ represent the dark matter density of the universe and g_*, g_{*s} represent the effective energy and entropy degrees of freedom. It is well-known that the formation of PBH shows exponential sensitivity to the tail of the Probability Distribution Function (PDF) of the density fluctuations where the non-Gaussian effects are prominent [244–249]. In the present scenario, there exist non-zero auto and cross-correlations between the two Gaussian random variables, $C_\mathcal{G}$ and ζ_G, which lead to the two-dimensional joint PDF:

$$\mathbb{P}_G(C_G,\zeta_G) = \frac{1}{2\pi\sigma_c\sigma_r\sqrt{1-\gamma_{\rm cr}^2}}\exp\left(-\frac{\zeta_G^2}{2\sigma_r^2}\right) \times\exp\left[\frac{-1}{2(1-\gamma_{\rm cr}^2)}\left(\frac{C_G}{\sigma_c}-\frac{\gamma_{\rm cr}\zeta_G}{\sigma_r}\right)^2\right], \tag{23}$$

with $\gamma_{cr} = \sigma_{cr}^2/(\sigma_c\sigma_r)$ representing the correlation coefficient. This PDF helps to calculate the required mass fraction of PBHs when considering the domain set by the threshold statistics on the compaction function (for details, see Appendix B) [205]:

$$\beta_{\rm NG}(M_H) = \int_{\mathcal{D}} \mathcal{K}(\mathcal{C}-\mathcal{C}_{\rm th})^\gamma \mathbb{P}_G(C_G,\zeta_G)dC_G\,d\zeta_G, \tag{24}$$

where the *critical scaling relation* is incorporated through $\mathcal{K}(\mathcal{C}-\mathcal{C}_{\rm th})^\gamma$ for the PBH mass formed during horizon re-entry [250,251]. The values for constant $\mathcal{K} \sim \mathcal{O}(1-10)$ and the threshold $\mathcal{C}_{\rm th}$, based on [233], arise from the simulations, and $\gamma \sim 0.36$ for the RD era. The integration domain is given by $\mathcal{D} = \{C(r) \geqslant \mathcal{C}_{\rm th} \wedge C_G(d\zeta/d\zeta_G) \leqslant 2u\}$, which involves maximizing the compaction function, the details for which we will provide in the SM. The 2D joint PDF contains various correlations for which we now provide the definitions [22,252]:

$$\sigma_{cr}^2 = \frac{2u}{3}\int_0^\infty \frac{dk}{k}(kr_m)^2 W_g(k,r_m)W_s(k,r_m)\tilde{\Delta}_\zeta^2(k), \tag{25}$$

$$\sigma_c^2 = \left(\frac{2u}{3}\right)^2\int_0^\infty \frac{dk}{k}(kr_m)^4 W_g^2(k,r_m)\tilde{\Delta}_\zeta^2(k), \tag{26}$$

$$\sigma_r^2 = \int_0^\infty \frac{dk}{k}W_s^2(k,r_m)\tilde{\Delta}_\zeta^2(k), \tag{27}$$

where we choose the smoothing functions, $W_g(k,r)$ and $W_s(k,r)$, to be Gaussian in nature, i.e., $\exp(-k^2r^2/2)$. The function $W_s(k,r)$ is referred to in the literature as the spherical-shell window function. For our purposes, we found that the choice of both such window functions to be Gaussian works well, rather than a top-hat and $W_s(k,r) = \sin(kr)/kr$ structure. This approach effectively smoothens small-scale fluctuations, and we will later observe its impact when evaluating the abundance of PBH in Fig. 3. We also used the smoothing property from the radiation transfer function, $T(k,\tau) = 3(\sin l - l\cos l)/l^3$, where $l = k\tau/\sqrt{3}$ and $\tau = 1/aH$, to define the new power spectrum form as $\tilde{\Delta}_\zeta^2(k) = T^2(k,r_m)\Delta_\zeta^2(k)$. Such use of the transfer function allows us to implement a damping effect, after going to the Fourier space, over the constantly evolving sub-horizon modes after they re-enter the horizon at scales $l = kc_s\tau \gg 1$. The structure of the transfer function tells us that in the sub-Horizon limit, $l \gg 1$, we have $T(k,\tau) = 0$, and for scales in the super-Horizon limit, $l \ll 1$, we have $T(k,\tau) = 1$ which makes it clear why the role of the transfer function remains valid only inside the Horizon and not on the super-Horizon mode evolution. It is important to note that eqns. (25)-(27) are evaluated at the horizon re-entry scale, $r_m = (\tilde{c_s}k_H)^{-1}$, which corresponds to the wavenumber during the formation of PBH and the scale where the compaction function maximizes. Soon as the threshold condition becomes satisfied, at $\tau = r_m$ the collapse of perturbations proceeds quickly and thus the modes which finally satisfy, $k \sim \mathcal{O}(r_m^{-1})$, lead to the dominant contributions towards PBH formation [236]. The relation between $\tilde{c_s}k_H \propto 1/\sqrt{M_H}$ [141,145] induces M_H dependence into the mass fraction, see appendix B.

Fig. 2 depicts contour plots of the 2D-PDF for different horizon mass values. In order to visualize the PDF, we use the eqn. (23). This formula shows that various correlation functions depend on the power spectrum amplitude, which we fix as $A = 10^{-2}$, the minimum value necessary to facilitate PBH production. The overall shape of the PDF depends on the set of such parameters. Although varying the power spectrum amplitude influences the PDF features, the amplitude is not directly fixed by the Gaussian variables C_G, ζ_G. However, the significance of the chosen amplitude comes into play when we set out to determine the domain of

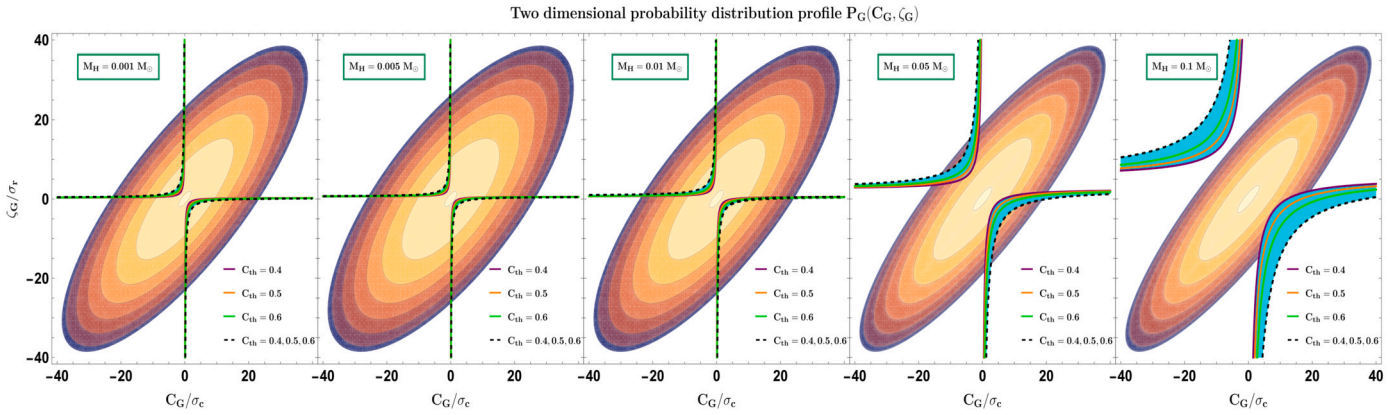

Fig. 2. Logarithmic plot of 2D PDF for various horizon mass M_H, including multiple values of the threshold density contrast, namely $\mathcal{C}_{\rm th} = 0.4, 0.5, 0.6$. $\mathbb{P}_G(\mathcal{C}_G, \zeta_G)$ is indicated by the contour lines plotted against the Gaussian variables: $\mathcal{C}_G, \zeta_G$. The shaded region between the two dotted lines indicates the parameter space, representing the integration domain to obtain a sizeable PBH mass fraction. All the plots are obtained for the scalar power spectrum having an amplitude $A = 10^{-2}$.

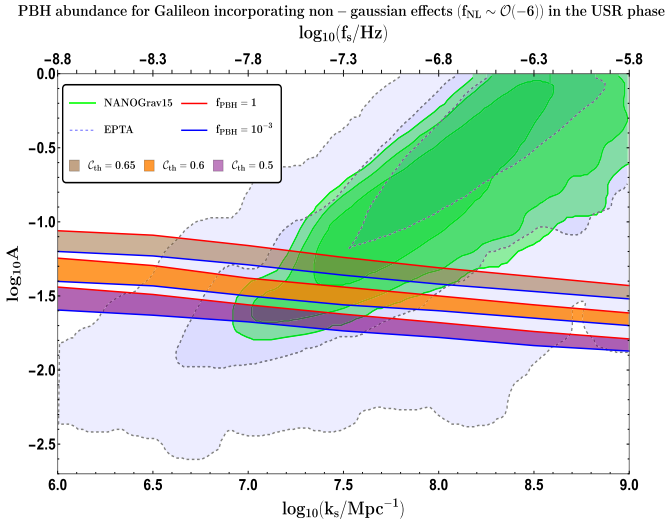

Fig. 3. PBH abundance from Galileon theory for different values of the volume-averaged density contrast threshold. The brown, orange, and purple coloured bands correspond to the threshold values in $\mathcal{C}_{\rm th} = \{0.65, 0.6, 0.5\}$, respectively. The red and blue borders of both bands bound the region of abundance $f_{\rm PBH} \in (1, 10^{-3})$. The green and light-blue posteriors representing, respectively, the NANOGrav 15 and EPTA are taken from [22].

integration, $\mathcal{D} = \{C(r) \geqslant \mathcal{C}_{th} \wedge C_G(d\zeta/d\zeta_G) \leqslant 2u\}$, which requires scaling the PDF points with the elements, σ_c, σ_r, in order to solve the inequalities for the Gaussian variables, $\mathcal{C}_G, \zeta_G$. The above domain $\mathcal{D}$ results from maximising the compaction function and on which more details are provided in appendix B. The purple, orange, and green coloured lines distinguish the allowed domains of integration for the mass fraction in eqn. (24). Each domain for a given threshold shares one common dashed black boundary with the respective colour for that threshold forming a complete integration region shaded in cyan. We observe that as the threshold on the compaction function, $\mathcal{C}_{\rm th}$, increases, the domain gets more squeezed and moves farther from the centre of the contour. The greater the support of the domain within the PDF, the greater the probability of having a sizeable abundance of that particular PBH mass, which is slightly less than the horizon mass at re-entry. The contours also show a notable behaviour where the quantity γ_{cr} increases as we go below, and also above, the mass, $M_H \sim \mathcal{O}(10^{-3} M_\odot)$, which signals large correlations between the two Gaussian variables. For masses with, $M_H > \mathcal{O}(0.1 M_\odot)$, the domain shows no overlap with the PDF, and thus it is much likely that the production of near solar mass PBHs is highly suppressed in our framework.

Before analyzing the results after computing PBH abundance, we clarify that throughout the remaining analysis, we follow the results in [233] on the interval of the threshold values. We maintain the underlying idea of only considering the NGs from the non-linearities in the compaction threshold at Horizon crossing. We elaborate on this with a discussion in the Appendix B.

Estimating the PBH abundance requires knowledge of the mass fraction and its allowed domain. We now analyze our results after using eqn. (22) as depicted in Fig. 3. The figure shows how large negative NG affects the PBH abundance, related to the transition wavenumbers k_s, by forcing the amplitude A of the scalar power spectrum in the USR to change for multiple choices of the compaction threshold. For $\mathcal{C}_{\rm th} = 0.65$, we observe that the no overproduction region (brown band and below) gets pushed towards larger amplitudes while maintaining the necessary perturbative approximation for the USR, $\Delta\mathcal{N}_{\rm USR} \sim \mathcal{O}(2)$, and where it begins to favour the SIGW interpretation of the NANOGrav15 data within 1σ. Upon changing the choice to $\mathcal{C}_{\rm th} = 0.6$, the region producing sizeable PBH abundance (orange band), $f_{\rm PBH} \in (1, 10^{-3})$, begins to fall in amplitude just outside the 1σ contour of the NANOGrav15 signal. Till now, we infer from the above that large NG, $f_{\rm NL} \sim \mathcal{O}(-6)$, tends to lessen the tension for extreme values of the compaction threshold in our theory. As we reach $\mathcal{C}_{\rm th} = 0.5$, PBH production increases further such that the region avoiding overproduction (purple band and below) moves down just close to the 2σ region. This behaviour is understandable, as increasing the threshold would require more amplitude to generate the same PBH mass. We must note here that the band decreases in amplitude for higher wavenumbers. Since the mass of PBH is related inversely to the transition wavenumber squared, smaller masses require a lesser amplitude of the power spectrum to generate a sizeable abundance.

We now turn our attention to the results where NG plays a crucial role in determining the power spectrum amplitude and the final fractional abundance of PBH. Fig. 4 compares the PBH abundance corresponding to distinct values of NG parameter, namely $f_{\rm NL} \in \{-2, -4, -6\}$ for a fixed threshold value of $\mathcal{C}_{\rm th} = 0.65$. It becomes clear that regardless of the change in $f_{\rm NL}$, there is no major statistical difference in the amplitude of the scalar power spectrum and, consequently, the corresponding PBH abundance. The values between the red lines correspond to $f_{\rm NL} = -6$, while the values between the blue and gray lines represent $f_{\rm NL} = -4$, and $f_{\rm NL} = -2$ respectively. All such bands lie within the 1σ contour of the NANOGrav15 and 2σ contour of the EPTA. The upper red lines lie closer to the 1σ contour than the blue and gray lines, indicating that the largest scalar power spectrum that can be obtained to get ideal abundance ($f_{\rm PBH} = 1$) is for $f_{\rm NL} = -6$. Upon analyzing, We will see a similar trend for other values of $\mathcal{C}_{\rm th}$, and this feature remains consistent with the results in Fig. 5. Thus, due to the value of $f_{\rm NL}$ only allowed to vary inside a finite interval for Galileon inflation, $-6 \leqslant f_{\rm NL} \leqslant -2$, leads to only a small change in the necessary peak amplitude A. Also,

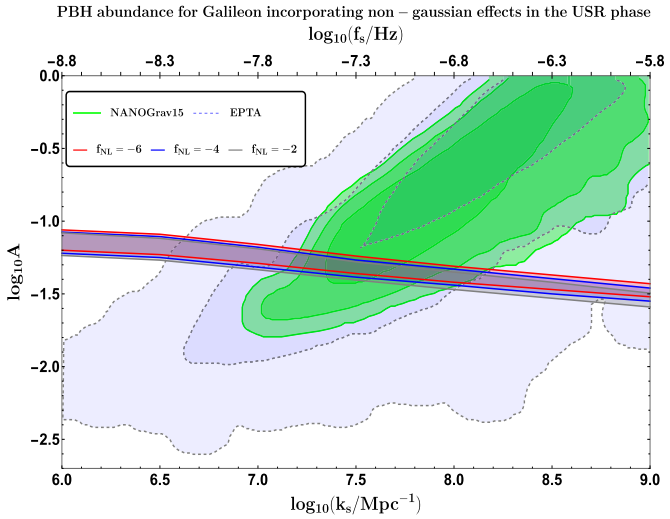

Fig. 4. PBH abundance from Galileon theory for different values of the non-Gaussianity measure, $f_{\rm NL} = -6$ (red), $f_{\rm NL} = -4$ (blue), $f_{\rm NL} = -2$ (gray), and a fixed compaction threshold, $\mathcal{C}_{\rm th} = 0.65$. In each band the PBH abundance belongs to the interval, $f_{\rm PBH} \in (1, 10^{-3})$. The green and light-blue posteriors representing, respectively, the NANOGrav 15 and EPTA.

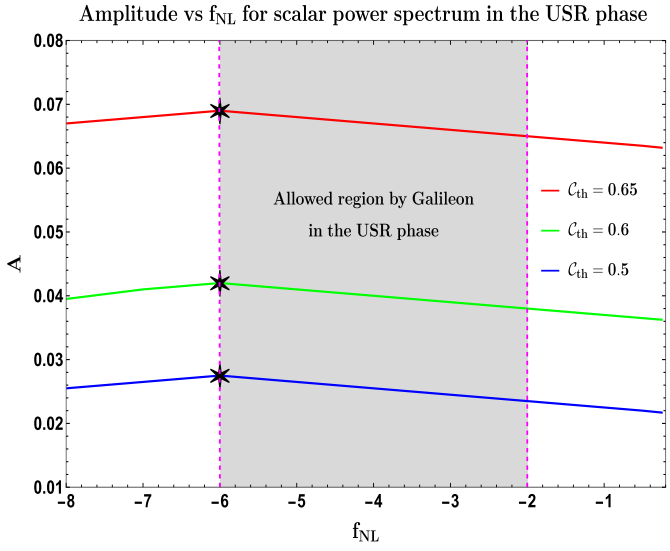

Fig. 5. Behaviour of the peak amplitude in the USR phase with changing values of negative NG, $f_{\rm NL}$. Different values of $\mathcal{C}_{\rm th} = \{0.65, 0.6, 0.5\}$ are considered and represented by red, green, and blue lines respectively, while the USR transition wavenumber $k_s = 10^7 {\rm Mpc}^{-1}$, and resulting fractional abundance $f_{\rm PBH} = 1$ is kept fixed. The black star represents the amplitude value corresponding to the maximum allowed abundance in the present conditions for $f_{\rm NL} = -6$. The gray shaded region with, $-6 \leqslant f_{\rm NL} \leqslant -2$, shows the theoretically allowed NG values in Galileon theory during the USR phase.

in the absence of any primordial NGs ($f_{\rm NL} = 0$) and just considering the impact of non-linearities, the SIGW interpretation of the NANOGrav15 signal breaks, and we will not obtain the desirable amplitude of the power spectrum as strictly proven in [22].

We next elaborate on the Fig. 5 that explores the impact of NGs on PBH abundance in a different manner. This plot depicts how the peak amplitude of the power spectrum, in the USR, changes for different values of local NG to achieve a maximum possible abundance. Large negative NG can seed large fluctuations that generate higher-mass black holes. Here, we have focused on the masses of PBH formed with the transition scale fixed at $k_s = 10^7 {\rm Mpc}^{-1}$. This scale allows for the generation of $M_{\rm PBH} \sim \mathcal{O}(10^{-2} M_\odot)$. As we tend to decrease $f_{\rm NL}$ below -6,

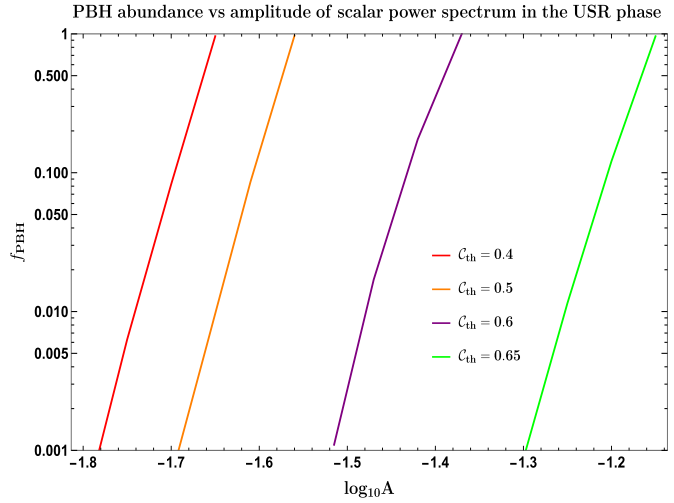

Fig. 6. Dependence of the PBH abundance on the scalar power spectrum amplitude of the curvature perturbation in the USR phase. The red, orange, blue, and green lines correspond to the threshold values of the compaction function, $\mathcal{C}_{\rm th} = \{0.4, 0.5, 0.6, 0.65\}$, respectively. The transition scale for this plot is fixed at $k_s = 10^7 {\rm Mpc}^{-1}$.

we observe that the amplitude in the USR falls to saturate the abundance of the said PBH masses. On the contrary, raising $f_{\rm NL}$ above -6 will increase the abundance of masses in the lower end of the allowed PBH mass spectrum, which then requires less amplitude for their formation. In the present context, Galileon theory does not allow for NG values outside the interval, $-6 \leqslant f_{\rm NL} \leqslant -2$, and the gray shaded region represents the theoretically allowed region. Throughout the analysis in Fig. 3, we have considered taking $f_{\rm NL} = -6$, its related power spectrum amplitudes shown using a black star marker for various thresholds, $\mathcal{C}_{\rm th} = \{0.5, 0.6, 0.65\}$, and this has provided us with the most satisfactory results for the agreement of the generated SIGWs with the PTA data.

After discussing the features of PBH abundance for various transition wavenumbers, including the impact of changing primordial NGs, we look at the sensitivity of $f_{\rm PBH}$ to the amplitude A more closely. In the Fig. 6 above, we can see how the amplitude changes for particular values of the compaction threshold to give rise to the fractional abundance in between the interval $f_{\rm PBH} \in (10^{-3}, 1)$, when we have fixed the transition scale $k_s = 10^7 {\rm Mpc}^{-1}$. As one can anticipate, increasing the threshold requires larger amplitudes of the scalar power spectrum to seed sizeable abundances of black holes. The plot also demonstrates that the abundance is highly sensitive to the amplitude, changing quickly and saturating to unity in an extremely short interval of the amplitude values. Here, we have kept the analysis within the mentioned regime of threshold values, $\mathcal{C}_{\rm th}$, where cosmological perturbation theory holds good.

From our examination of the abundance of PBH, we observe that unlike working with a two-field model, like the curvaton, for generating the PBH forming curvature perturbations, the single-field Galileon theory employs an additional USR feature during inflation, whose duration respects the established perturbativity conditions [19,212,213]. It sufficiently enhances the scalar power spectrum for PBH formation and contributes towards the overall quantum one-loop corrections. The resulting amplitude corresponds to sizeable PBH abundance without risking overproduction. The analysis done for the curvaton model in [22,205] considers the NGs in great detail to obtain a suitable abundance and thus leads to the amplitude of the power spectrum that is enough to alleviate the tension between NANOGrav 15 and SIGWs. On the other hand, Galileon further includes larger negative NGs such that the resulting amplitude generates the SIGWs that correlate strongly with NANOGrav 15 data in the presence of the quantum loop effects.

In this letter, we have utilized the threshold statistics on the compaction function, which helps us to consider the primordial NGs and the inbuilt non-linearities into the density contrast field. We first demonstrated that the SIGW spectra corresponding to $c_s = \{0.04, 0.05, 0.06\}$ comply well with the NANOGrav 15 and EPTA signal. Accompanying this, with the NG value of $f_{\rm NL} \sim \mathcal{O}(-6)$, we obtained sizeable PBH abundance in the range $f_{\rm PBH} \in (10^{-3} - 1)$ which manages to remove the overproduction problem. We conclude that large negative NGs within Galileon theory, which come from respecting the perturbativity conditions on the USR phase, allow for a sizeable PBH abundance and consequently lead to the amplitude of scalar power spectrum that conforms within 2σ to the SIGW interpretation of the observed GW signal from the PTA collaborations.

Declaration of competing interest

The authors declare that they have no known competing financial interests or personal relationships that could have appeared to influence the work reported in this paper.

Data availability

No data was used for the research described in the article.

Acknowledgements

SC would like to thank The National Academy of Sciences (NASI), Prayagraj, India for being elected as a member of the academy. SP is supported by the INSA Senior scientist position at NISER, Bhubaneswar through the Grant number INSA/SP/SS/2023. MS is supported by Science and Engineering Research Board (SERB), DST, Government of India under the Grant Agreement number CRG/2022/004120 (Core Research Grant). MS is also partially supported by the Ministry of Education and Science of the Republic of Kazakhstan, Grant No. 0118RK00935, and CAS President's International Fellowship Initiative (PIFI).

Appendix A. Details for the scalar power spectrum

In this section we focus on building the comoving curvature perturbation mode solutions once we obtain the corresponding equation of motion for the curvature perturbation from the second-order action presented in eqn. (3). Redefining the action in terms of a new variable, z, helps us to give the resulting equation of motion:

$$\zeta_{\mathbf{k}}''(\tau) + 2\frac{z'(\tau)}{z(\tau)}\zeta_{\mathbf{k}}'(\tau) + c_s^2 k^2 \zeta_{\mathbf{k}}(\tau) = 0,$$
$$\text{where} \quad z(\tau) = a\sqrt{2\mathcal{A}}/H^2, \tag{A.1}$$

with this equation in hand, we can proceed towards analyzing the mode solutions and the related power spectrum functions in different phases during inflation in our theory.

The power spectrum receives contributions from each SRI, USR, and SRII phase. However, we encounter a different set of Bogoliubov coefficients for each phase after solving the Israel junction conditions for the curvature perturbation modes. These new coefficients correctly describe the mode solutions of the new phase, including the properties of the respective quantum vacuum state. The mode solutions, along with their corresponding Bogoliubov coefficients for each phase, are listed below. We introduce the following shorthand notations for the sake of convenience while writing the mentioned mode solutions and coefficients:

$$f_{\pm,\mathbf{k}}(\tau) = \left(\frac{iH^2}{2\sqrt{\mathcal{A}}}\right)\frac{1}{(c_s k)^{3/2}} \times (1 \pm ikc_s\tau)\exp(\mp ikc_s\tau),$$
$$\mathcal{X}_s \equiv k/k_s, \qquad \mathcal{X}_e \equiv k/k_e, \tag{A.2}$$

where, $|\mathbf{k}| = k$, denotes the magnitude of the wavenumber.

(a) **For the SRI phase:** The following expression represents the solution for the scalar mode corresponding to the SRI phase where the conformal time satisfies the condition, $\tau < \tau_s$:

$$\zeta_{\mathbf{k}}(\tau) = \left[\alpha_{\mathbf{k}}^{(1)} f_{+,\mathbf{k}}(\tau) - \beta_{\mathbf{k}}^{(1)} f_{-,\mathbf{k}}(\tau)\right]. \tag{A.3}$$

The Bogoliubov coefficients involved in the above solution have the following values:

$$\alpha_{\mathbf{k}}^{(1)} = 1, \qquad \beta_{\mathbf{k}}^{(1)} = 0. \tag{A.4}$$

This choice of coefficients indicates use of the well-studied Bunch-Davies quantum vacuum state as our starting point.

(b) **For the USR phase:** The following expression represents the solution for the scalar mode corresponding to the USR phase where the conformal time satisfies the condition, $\tau_s \leqslant \tau < \tau_e$:

$$\zeta_{\mathbf{k}}(\tau) = \left(\frac{\tau_s}{\tau}\right)^3 \left[\alpha_{\mathbf{k}}^{(2)} f_{+,\mathbf{k}}(\tau) - \beta_{\mathbf{k}}^{(2)} f_{-,\mathbf{k}}(\tau)\right]. \tag{A.5}$$

The Bogoliubov coefficients involved in the above solution have the following values:

$$\alpha_{\mathbf{k}}^{(2)} = 1 + \frac{3}{2i\mathcal{X}_s^3}\left(1 + \mathcal{X}_s^2\right),$$
$$\beta_{\mathbf{k}}^{(2)} = \frac{3}{2i\mathcal{X}_s^3}\left(1 - i\mathcal{X}_s^2\right)^2 \exp\left(2i\mathcal{X}_s\right). \tag{A.6}$$

To obtain the above we require applying the continuity of the mode solutions and its conjugate momenta in SRI and USR at the transition scale k_s.

(c) **For the SRII phase:** The following expression represents the solution for the scalar mode corresponding to the SRII phase where the conformal time satisfies the condition, $\tau_e \leqslant \tau \leqslant \tau_{\rm end}$:

$$\zeta_{\mathbf{k}}(\tau) = \left(\frac{\tau_s}{\tau_e}\right)^3 \left[\alpha_{\mathbf{k}}^{(3)} f_{+,\mathbf{k}}(\tau) - \beta_{\mathbf{k}}^{(3)} f_{-,\mathbf{k}}(\tau)\right]. \tag{A.7}$$

The Bogoliubov coefficients involved in the above solution have the following values:

$$\alpha_{\mathbf{k}}^{(3)} = -\frac{1}{4\mathcal{X}_s^3\mathcal{X}_e^3}\Bigg[9\left(-\mathcal{X}_e + i\right)^2\left(\mathcal{X}_s + i\right)^2\exp\left(2i\left(\mathcal{X}_s - \mathcal{X}_e\right)\right)$$
$$+ \left\{\mathcal{X}_e^2\left(2\mathcal{X}_e + 3i\right) + 3i\right\}\left\{\mathcal{X}_s^2\left(-2\mathcal{X}_s + 3i\right) + 3i\right\}\Bigg], \tag{A.8}$$

$$\beta_{\mathbf{k}}^{(3)} = \frac{3}{4\mathcal{X}_s^3\mathcal{X}_e^3}\Bigg[\left(\mathcal{X}_s + i\right)^2\left\{\mathcal{X}_e^2\left(2i\mathcal{X}_e + 3\right)\right\}\exp\left(2i\mathcal{X}_s\right)$$
$$+ i\left(\mathcal{X}_e + i\right)^2\left\{3i + \mathcal{X}_s^2\left(-2\mathcal{X}_s + 3i\right)\right\}\exp\left(2i\mathcal{X}_e\right)\Bigg]. \tag{A.9}$$

In order to obtain the above we require applying the continuity of the mode solutions and its conjugate momenta in USR and SRII at the transition scale k_e.

From using the above information, one can able to write the final scalar power spectrum which includes the tree-level and the one-loop contributions in terms of the wavenumber as:

$$\Delta^2_{\zeta,\mathbf{Total}}(k) = \left[\Delta^2_{\zeta,\mathbf{Total}}(k)\right]_{\mathbf{SRI}} + \left[\Delta^2_{\zeta,\mathbf{Total}}(k)\right]_{\mathbf{USR}}\Theta(k - k_s)$$
$$+ \left[\Delta^2_{\zeta,\mathbf{Total}}(k)\right]_{\mathbf{SRII}}\Theta(k - k_e),$$
$$= \left[\Delta^2_{\zeta,\mathbf{Tree}}(k)\right]_{\mathbf{SRI}}\Bigg\{1 + \left(\frac{k_e}{k_s}\right)^6\Bigg(\left|\alpha_{\mathbf{k}}^{(2)} - \beta_{\mathbf{k}}^{(2)}\right|^2\Theta(k - k_s)$$
$$+ \left|\alpha_{\mathbf{k}}^{(3)} - \beta_{\mathbf{k}}^{(3)}\right|^2\Theta(k - k_e)\Bigg) + \mathcal{Q}_c\Bigg\},$$

$$= A\left[1+\mathcal{X}_s^2\right]\left\{\left(\frac{k_s}{k_e}\right)^6(1+\mathcal{Q}_c) + \left(\left|\alpha_{\mathbf{k}}^{(2)}-\beta_{\mathbf{k}}^{(2)}\right|^2\Theta(k-k_s)+\left|\alpha_{\mathbf{k}}^{(3)}-\beta_{\mathbf{k}}^{(3)}\right|^2\Theta(k-k_e)\right)\right\}, \tag{A.10}$$

where we have used the following definitions:

$$\left[\Delta^2_{\zeta,\mathbf{Tree}}(k)\right]_{\mathbf{SRI}} = \left(\frac{H^4}{8\pi^2\mathcal{A}c_s^3}\right)_*\left[1+\mathcal{X}_s^2\right], \qquad A = \left(\frac{H^4}{8\pi^2\mathcal{A}c_s^3}\right)_*\left(\frac{k_e}{k_s}\right)^6, \tag{A.11}$$

and the term labelled $\mathcal{Q}_c$ represents the collection of the one-loop quantum corrections from each phase. For more details on the explicit computation of these one-loop contributions in Galileon theory, see ref. [212]. Also, aside from the Bogoliubov coefficients for each phase which includes the sharp transition wavenumbers, the total scalar power spectrum from Galileon theory takes in the effective sound speed c_s, and the time-dependent coefficients obtained before for the second-order action in eqns. (4), (5).

Appendix B. Compaction function and its threshold statistics

This section details the necessary computations when applying the threshold statistics to the compaction function. First introduced by Shibata and Sasaki in [253], this function is defined to be twice the excess mass over the areal radius:

$$C(r,t) = 2\times\left(\frac{M(r,t)-M_o(r,t)}{R(r,t)}\right) = \frac{2}{R(r,t)}\int_{S_R^2} d^3\vec{x}\,\rho_o(t)\delta(\vec{x},t), \tag{B.1}$$

where $M_o(r,t)=\rho_0(t)V_o(r,t)$, with $V_o(r,t)=(4\pi/3)R(r,t)^3$, denotes the background mass with respect to the energy density $\rho_o(t)$, and $M(r,t)$ denotes the Misner-Sharp mass within the sphere S_R^2 of areal radius, $R(r,t)\equiv a(t)r\exp(\zeta(r))$, written in the comoving radial coordinates. Now, upon analyzing the perturbations well outside the cosmological horizon, one can accommodate the non-linearities from the conserved curvature perturbation, $\zeta(r)$, into the density contrast field $\delta(\vec{x},t)=\delta\rho(\vec{x},t)/\rho_o(t)$ by using the long-wavelength approximation (also known as the gradient expansion) on such super-horizon scales. For a generic background with the equation of state w, the above-mentioned non-linearities in the radial coordinates result from the expression [236,254]:

$$\delta(r,t) = -\frac{2u}{3}\left(\frac{1}{aH}\right)^2 e^{-5\zeta(r)/2}\nabla^2 e^{\zeta(r)/2}, \approx -\frac{2u}{3}\frac{1}{(aH)^2}e^{-2\zeta(r)}\left[\zeta''(r)+\frac{2}{r}\zeta'(r)+\frac{1}{2}\zeta'(r)^2\right], \tag{B.2}$$

where $u=3(1+w)/5+3w$ and a prime indicates a radial derivative. The analysis performed in this letter is not restricted to any particular component but can be generalized to any equation of state, along with Galileon, within $0\leqslant w\leqslant 1$, which covers $w=\{0,1/3,1\}$ describing the matter-dominated, radiation dominated, and the kination era respectively. In the above equation, the Laplacian in radial coordinates and the exponential terms introduce the explicit non-linear effects, which makes it clear that NGs will inevitably be present regardless of the statistics of the curvature perturbation $\zeta(r)$ [235,255]. Using the non-linear eqn. (B.2), the compaction function in eqn. (B.1) achieves the new time-independent definition:

$$C(r) = -2ur\zeta'(r)\left(1+\frac{r}{2}\zeta'(r)\right). \tag{B.3}$$

The above equation can be separated into its linear and non-linear components as follows:

$$C(r) = C_{\rm L}(r) - C_{\rm NL}(r) \quad \text{where,}$$
$$C_{\rm L}(r) = -2ur\zeta'(r), \quad \text{and} \quad C_{\rm NL}(r) = C_{\rm L}(r)^2/4u. \tag{B.4}$$

Now, the criterion for the PBH formation comes from maximizing the compaction function at the scale r_m, which, on using the eqn. (B.3), enables the condition:

$$\zeta'(r_m) + r_m\zeta''(r_m) = 0. \tag{B.5}$$

The same comoving scale r_m can as well be associated to the Horizon mass M_H through the standard relation in terms of the corresponding wavenumbers, $\tilde{c_s}k_H = r_m^{-1}$, that source the PBH forming perturbation during horizon re-entry (crossing):

$$M_H \approx 17M_\odot\left[\frac{g_*}{10.75}\right]^{-1/6}\left[\frac{\tilde{c_s}k_H}{10^6\text{Mpc}^{-1}}\right]^{-2}. \tag{B.6}$$

where $g^*=106.75$ represents the relativistic d.o.f. in the radiation-dominated epoch, and, in the present scenario, k_H corresponds to the transition scale k_s into the USR region. We incorporate the effective sound speed at the transition scale by using $\tilde{c_s}\approx 1\pm\delta$, such that $\delta\ll 1$. At this stage, let's also examine the excess mass volume-averaged over a region with areal radius R. This quantity has a special relation at the scale r_m, and the corresponding re-entry time t_H, with the compaction function at the same scale:

$$\delta_m = \frac{\delta M(r,t)}{M_o(r,t)} \equiv \frac{3}{R_m}\int_0^{R_m}\frac{\delta\rho}{\rho_o}R^2\,dR = C(r_m) = 3\delta(r_m,t_H), \tag{B.7}$$

in the above, $R_m = a(t_H)r_m e^{\zeta(r_m)}$, is the physical length scale of the perturbation during re-entry. The last two equalities are realised only after the use of the Horizon crossing condition $R_m H(t_H)=1$, the eqn. (B.2), and the condition in eqn. (B.5) in above while considering eqn. (B.3). The eqn. (B.7) is a significant result, as it directly brings the volume-averaged density contrast, δ_m, into the picture through the compaction function at horizon re-entry.

Current estimates for the volume-averaged density contrast on super-horizon scales, obtained using numerical analysis, result in the interval, $2/5\leqslant\delta_{\rm th}\leqslant 2/3$, where under the first approximation, that is neglecting higher-order effects in the gradient expansion approach, is said to provide a reasonable outcome for the perturbation amplitude during horizon re-entry [233,236] at the associated scale r_m and the perturbation mode k_H. An important fact to remember here is that in the mentioned studies, only the NG effects due to the non-linearities from eqn. (B.2) are taken into account, along with assuming that the curvature perturbation only follows Gaussian statistics to give us the above interval for $\delta_{\rm th}$. Recent studies in [234,256] have looked into the effects of quadratic primordial NGs on the computation of the threshold and found changes only at a few percent level. Through the equality in eqn. (B.7), we can then directly determine the range of the threshold values $C_{\rm th}$.

We now discuss briefly the approaches adopted by different studies to incorporate the impact of $f_{\rm NL}$ on the compaction threshold estimation. The study in [256] makes it clear, through the use of a curvature perturbation profile, that the volume-averaged compaction function approach with its universal threshold value of $\bar{C}=2/5$, only works well for models with positive $f_{\rm NL}$ and fails for the cases where negative $f_{\rm NL}\lesssim -1$. To thoroughly determine the compaction threshold for a specific model would require using a curvature perturbation profile, ζ_G, and dedicated simulations on the behaviour of the compaction function, which shows the resulting impact coming from the presence of quadratic NGs. The curvature perturbations will also then experience changes with the new threshold values for different values of $f_{\rm NL}$ and go on to directly

affect the PBH formation process. Otherwise, one can also follow the relatively new path-integral techniques followed by [234] where they employ threshold statistics to study non-Gaussian corrections to the curvature perturbation correlations and their impact on the average density perturbation profile. For this work, we avoid this entirely separate study of estimating the threshold and follow the volume-averaged compaction threshold prescription as laid in [233]. For our analysis, we do not begin by assuming a template expression for the Gaussian curvature perturbation and rely on the various correlations and their joint PDF to get the set of values for the variables, $\mathcal{C}_G, \zeta_G$. We then use the horizon crossing property to identify the two quantities, $\delta_m = \mathcal{C}(r_m)$, and get the threshold $\mathcal{C}_{\rm th}$ to ultimately perform the integration over the complete domain satisfying specific conditions which we can now begin to examine.

Since we are considering a generic expression for the curvature perturbation $\zeta(r)$ which carries within the primordial NG information, this also appears inside the equation (B.3), which we now mention as:

$$\mathcal{C}(r) = \mathcal{C}_G(r)\frac{d\zeta}{d\zeta_G} - \frac{1}{4u}\left(\mathcal{C}_G(r)\frac{d\zeta}{d\zeta_G}\right)^2, \tag{B.8}$$

with $\mathcal{C}_G(r) = -2ur\zeta_G'(r)$. The conditions under which a cosmological perturbation undergoes collapse to form PBH get decided by, firstly, requiring the condition $\mathcal{C} \geqslant \mathcal{C}_{\rm th}$, based on the threshold of the compaction function $\mathcal{C}_{\rm th}$. While this is true, maximizing the compaction function sets another boundary condition to provide us with a proper domain of values:

$$\begin{aligned}
\mathcal{C}'(r) &= \mathcal{C}_{\rm L}'(r) - \mathcal{C}_{\rm NL}'(r) = \mathcal{C}_{\rm L}'(r) - \frac{d}{dr}\left(\frac{\mathcal{C}_{\rm L}(r)^2}{4u}\right), \\
&= \mathcal{C}_{\rm L}'(r) - \frac{1}{2u}\left(\mathcal{C}_{\rm L}(r)\,\mathcal{C}_{\rm L}'(r)\right) = 0, \\
\implies \mathcal{C}_{\rm L}(r) &= 2u.
\end{aligned} \tag{B.9}$$

Finding a double derivative gives an affirmative over the second boundary condition as being, $\mathcal{C}_{\rm L}(r) \leq 2u$ or $\mathcal{C}_G(d\zeta/d\zeta_G) \leqslant 2u$. As a result, the complete domain for integrating the PBH mass fraction after the use of threshold statistics on the compaction function reads: $\mathcal{D} = \{\mathcal{C}(r) \geqslant \mathcal{C}_{th} \wedge \mathcal{C}_G(d\zeta/d\zeta_G) \leqslant 2u\}$.

Appendix C. Primordial non-Gaussianity and PBH mass fraction

Including NG in the comoving curvature perturbation is essential due to the presence of a USR phase during inflation. Now, the NG corrections are suppressed at the CMB scales due to the small values of the slow-roll parameters. However, the introduction of a USR phase contributes significantly to the NGs. In this section, we elaborate on the effects of deviating from the Gaussian limit due to considering the local type of primordial NGs in the curvature perturbations. Specifically, we are considering the quadratic parameterization of the perturbation, $\zeta = \zeta_G + (3/5)f_{\rm NL}\zeta_G^2$, in terms of the Gaussian random variable ζ_G.

Starting with the already discussed 2D joint PDF in eqn. (23), we ask how deviating from a perfectly correlated scenario, where one essentially considers a Dirac delta type of distribution, brings changes into the results of the primordial abundance of black holes. Upon Taylor expanding the existing PDF in between the 2 Gaussian variables, $\mathcal{C}_G, \zeta_G$, around the value of $\gamma_{cr} = 1$, we can get the following expression:

$$\begin{aligned}
\mathbb{P}_G(\mathcal{C}_G, \zeta_G) = \frac{1}{2\sqrt{2}\pi\sigma_c\sigma_r\sqrt{1-\gamma_{cr}}} \exp\left(\frac{1}{4(\gamma_{cr}-1)}\left(\frac{\mathcal{C}_G}{\sigma_c} - \frac{\zeta_G}{\sigma_r}\right)^2\right. \\
\left. + \sum_{n=3}^{\infty}\left(\frac{-1}{2}\right)^n\left(\frac{\mathcal{C}_G}{\sigma_c} + \frac{\zeta_G}{\sigma_r}\right)^2(\gamma_{cr}-1)^{n-3}\right) \\
\times\left(1 + \frac{1-\gamma_{cr}}{4} + \frac{3(1-\gamma_{cr})^2}{32} + \frac{5(1-\gamma_{cr})^3}{128} + \frac{35(1-\gamma_{cr})^4}{2048}\right. \\
\left. + \frac{63(1-\gamma_{cr})^5}{8192} + \frac{231(1-\gamma_{cr})^6}{65536} + \cdots\right),
\end{aligned} \tag{C.1}$$

where the $\cdots$ represent the higher-order terms in the Taylor expansion and, under the particular limit $\gamma_{cr} \to 1$, the above distribution reduces to as follows:

$$\begin{aligned}
\lim_{\gamma_{cr}\to 1}\mathbb{P}_G(\mathcal{C}_G, \zeta_G) &= \frac{1}{\sqrt{2\pi}\sigma_c\sigma_r}\exp\left(-\frac{1}{8}\left(\frac{\mathcal{C}_G}{\sigma_c} + \frac{\zeta_G}{\sigma_r}\right)^2\right) \\
&\times \lim_{\gamma_{cr}\to 1}\frac{1}{\sqrt{2\pi(2(1-\gamma_{cr}))}}\exp\left(\frac{1}{4(\gamma_{cr}-1)}\left(\frac{\mathcal{C}_G}{\sigma_c} - \frac{\zeta_G}{\sigma_r}\right)^2\right), \\
&= \frac{1}{\sqrt{2\pi}\sigma_c\sigma_r}\exp\left(-\frac{1}{8}\left(\frac{\mathcal{C}_G}{\sigma_c} + \frac{\zeta_G}{\sigma_r}\right)^2\right)\delta\left(\frac{\mathcal{C}_G}{\sigma_c} - \frac{\zeta_G}{\sigma_r}\right) \quad .
\end{aligned} \tag{C.2}$$

Here the Dirac delta function enforces the condition, $\mathcal{C}_G/\sigma_c = \zeta_G/\sigma_r$, in the remaining quadratic expression reducing it down to a sharp or highly correlated distribution function, which must be the case since the correlation coefficient γ_{cr} reaches to its maximum value of $\gamma_{cr} = 1$. The expansion in eqn. (C.1) is only valid when the distribution is in the vicinity of being highly correlated and is infinitely differentiable, which seems to be the case here, or else the series expansion breaks for lower values of γ_{cr}. In the present context, the Fig. 2 featuring the contour plots have the value of the correlation coefficient satisfying $0.84 \lesssim \gamma_{cr} < 1$ for $M_H \geqslant 10^{-3}M_\odot$ and thus justifies performing such an expansion. The resulting additional terms will contribute to the overall PBH mass fraction and the corresponding fractional abundance, in addition to the contribution from the sharply peaked distribution.

Given the peaked distribution in eqn. (C.2), its contribution to the total mass fraction can be written as:

$$\begin{aligned}
\beta_{\rm peak}(M_H) &= \frac{1}{\sqrt{2\pi}\sigma_c\sigma_r}\int_{\mathcal{D}} d\mathcal{C}_G\, d\zeta_G\, \mathcal{K}(\mathcal{C} - \mathcal{C}_{\rm th})^\gamma \\
&\times \exp\left(-\frac{1}{8}\left(\frac{\mathcal{C}_G}{\sigma_c} + \frac{\zeta_G}{\sigma_r}\right)^2\right)\delta\left(\frac{\mathcal{C}_G}{\sigma_c} - \frac{\zeta_G}{\sigma_r}\right), \\
&= \frac{1}{\sqrt{2\pi}\sigma_r}\int_{\mathcal{D}} \mathcal{K}\left\{\left[g(\zeta_G) - \frac{1}{4u}g(\zeta_G)^2\right] - \mathcal{C}_{\rm th}\right\}^\gamma \\
&\times \exp\left(-\frac{\zeta_G^2}{2\sigma_r^2}\right)d\zeta_G.
\end{aligned} \tag{C.3}$$

Due to the Dirac delta function, one obtains an integral over the variable ζ_G where we define the function $g(\zeta_G) = \frac{\sigma_c}{\sigma_r}\zeta_G\frac{d\zeta}{d\zeta_G}$ for convenience. The remaining constants, $\{\mathcal{K}, u, \mathcal{C}_{\rm th}, \gamma\}$, are the same as defined previously during the first appearance of the joint PDF. This PBH mass fraction further enables the computation of the related fractional abundance after integration over a range of horizon masses, which label here the possible epochs of black hole formation. The abundance corresponding to the peak distribution is derived through the following expression:

$$\begin{aligned}
f_{\rm PBH}^{\rm peak} \equiv \frac{\Omega_{\rm PBH}^{\rm peak}}{\Omega_{\rm DM}} &= \frac{1}{\Omega_{\rm DM}}\int d\ln M_H\left(\frac{M_H}{M_\odot}\right)^{-1/2} \\
&\times \left(\frac{g_*}{106.75}\right)^{3/4}\left(\frac{g_{*s}}{106.75}\right)^{-1}\left(\frac{\beta_{\rm peak}(M_H)}{7.9\times 10^{-10}}\right).
\end{aligned} \tag{C.4}$$

In the above the time-dependent horizon mass contained within the Universe of radius $1/H(t)$ at cosmic time t is defined as $M_H \equiv M_H(t) = (4\pi/3)\rho(t)/H^3(t)$, with $\rho(t)$ being the total energy density of the Universe at the same time and $\Omega_{\rm DM} \simeq 0.264$ corresponds to the dark matter density of the Universe. The Gaussian PDF in the above calculation is responsible for getting the maximum possible contribution to the total abundance. The rest of the terms providing deviation from Gaussian nature in the PDF expansion provide smaller contributions to the total mass fraction and consequently result in an estimate of the fractional abundance, which changes less significantly, especially for the values of correlation coefficient, γ_{cr}, in our case. This analysis tells us that the

fractional abundance is not highly sensitive to other terms in the PDF expansion, in contrast to the primordial NGs, which determine the domain and the scalar power spectrum amplitude, which is present inside the variances and gives rise to an exponential sensitivity to the fractional abundance.

We now present some general discussions regarding our analysis based on the non-linearities, NGs, and the necessary perturbativity conditions,

- **Inclusion of non-linearities**: The broad analysis done in this letter does not ignore the apparent non-linearities in the density contrast field inherited from the possible non-linear behaviour of the curvature perturbations on super-horizon scales. We chose the compaction function as it provides a much better estimate for the formation threshold of the density contrast in the presence of the non-linear modifications [233,236]. In this work, we have utilized this estimate to evaluate the PBH mass fraction using the critical scaling relation and the integration domain dependent on the threshold value and the impacts induced by non-linearities. These non-linearities also do not tend to overpower their effects and become uncontrollable, which is visible in our previous results including the analysis of the Figs. 5-6.
- **Effects of non-Gaussianities**: These originate in our present analysis from two essential places. The first comes through the non-linearities in the density contrast field from where the non-Gaussian effects propagate, even when one assumes Gaussian statistics for the curvature perturbation. The second is connected with the generation of PBHs, where slow-roll violation for a brief period occurs to sufficiently enhance the scalar power spectrum amplitude. One must include these sources for a more realistic analysis of the PBH formation and their fractional abundance for the present-day total dark matter content. The local primordial NGs are present inside our use of the quadratic model for the curvature perturbation, which then gets translated into the compaction function. The amount of NG ($f_{\rm NL}$) present, hence, ultimately controls the scalar power spectrum amplitude and the PBH abundance, which will be elaborated on, shortly in the results of this section.
- **Preserving perturbativity**: In our setup, a USR phase to generate the large curvature perturbations comes with certain conditions imposed on its period. We have maintained throughout our analysis the critical condition on the e-foldings of the USR, $\Delta\mathcal{N}_{\rm USR} \sim \mathcal{O}(2)$ which guarantee that the cosmological perturbative approximations and controlled production of NGs are both satisfied. Another necessary perturbative approximation follows while restricting our analysis for the volume-averaged density contrast threshold to, $2/5 \leqslant \delta_{\rm th} \leqslant 2/3$, which is the same for the compaction threshold $\mathcal{C}_{\rm th}$ at the time of horizon crossing. In this window, non-linear effects present during the long-wavelength approximation on super-horizon scales remain controllable. The upcoming discussions on our results will show that preserving perturbativity brings about satisfactory outcomes.
- **Respecting Causality and Unitarity**: The effective sound speed parameter, c_s, takes on a conformal time-dependent behaviour in our present setup. Its value at the pivot scale is given by $c_s(\tau_*) = c_s$, where τ_* is the conformal time for the pivot scale $k_* = 0.02{\rm Mpc}^{-1}$. During our analysis of the SIGWs generated from Galileon theory, the properties of unitarity and causality have been preserved by satisfying the observational constraint, $0.024 \leqslant c_s < 1$, [257].
- **Mass of PBH and NGs**: PBH formation requires a brief period of slow-roll violation, which, in the present context, is introduced through a USR phase. Specifically, the wavenumber associated with the transition from the slow-roll to the USR phase, k_s, is the crucial parameter determining the resulting mass of the PBH. The dependency goes as $\tilde{c_s} k_s \propto 1/\sqrt{M_{\rm PBH}}$. Regardless of the exact position of the USR, large enhancements in the NGs remain present in our setup. In this work, we have set the transition scale at $k_s = 10^7{\rm Mpc}^{-1}$, which corresponds to the formation of $M_{\rm PBH} \sim \mathcal{O}(0.01) M_\odot$, and additionally generates large negative NGs [213].

References

[1] NANOGrav Collaboration, G. Agazie, et al., The NANOGrav 15 yr data set: evidence for a gravitational-wave background, Astrophys. J. Lett. 951 (1) (2023) L8, arXiv:2306.16213 [astro-ph.HE].
[2] NANOGrav Collaboration, G. Agazie, et al., The NANOGrav 15 yr data set: observations and timing of 68 millisecond pulsars, Astrophys. J. Lett. 951 (1) (2023) L9, arXiv:2306.16217 [astro-ph.HE].
[3] NANOGrav Collaboration, G. Agazie, et al., The NANOGrav 15 yr data set: detector characterization and noise budget, Astrophys. J. Lett. 951 (1) (2023) L10, arXiv:2306.16218 [astro-ph.HE].
[4] NANOGrav Collaboration, A. Afzal, et al., The NANOGrav 15 yr data set: search for signals from new physics, Astrophys. J. Lett. 951 (1) (2023) L11, arXiv:2306.16219 [astro-ph.HE].
[5] NANOGrav Collaboration, G. Agazie, et al., The NANOGrav 15 yr data set: constraints on supermassive black hole binaries from the gravitational-wave background, Astrophys. J. Lett. 952 (2) (2023) L37, arXiv:2306.16220 [astro-ph.HE].
[6] NANOGrav Collaboration, G. Agazie, et al., The NANOGrav 15-year data set: search for anisotropy in the gravitational-wave background, arXiv:2306.16221 [astro-ph.HE].
[7] NANOGrav Collaboration, G. Agazie, et al., The NANOGrav 15 yr data set: Bayesian limits on gravitational waves from individual supermassive black hole binaries, Astrophys. J. Lett. 951 (2) (2023) L50, arXiv:2306.16222 [astro-ph.HE].
[8] NANOGrav Collaboration, A.D. Johnson, et al., The NANOGrav 15-year gravitational-wave background analysis pipeline, arXiv:2306.16223 [astro-ph.HE].
[9] EPTA Collaboration, J. Antoniadis, et al., The second data release from the European pulsar timing array III. Search for gravitational wave signals, arXiv:2306.16214 [astro-ph.HE].
[10] EPTA Collaboration, J. Antoniadis, et al., The second data release from the European pulsar timing array I. The dataset and timing analysis, arXiv:2306.16224 [astro-ph.HE].
[11] EPTA Collaboration, J. Antoniadis, et al., The second data release from the European pulsar timing array II. Customised pulsar noise models for spatially correlated gravitational waves, arXiv:2306.16225 [astro-ph.HE].
[12] EPTA Collaboration, J. Antoniadis, et al., The second data release from the European pulsar timing array IV. Search for continuous gravitational wave signals, arXiv:2306.16226 [astro-ph.HE].
[13] EPTA Collaboration, J. Antoniadis, et al., The second data release from the European pulsar timing array: V. Implications for massive black holes, dark matter and the early universe, arXiv:2306.16227 [astro-ph.CO].
[14] EPTA Collaboration, C. Smarra, et al., The second data release from the European pulsar timing array: VI. Challenging the ultralight dark matter paradigm, arXiv:2306.16228 [astro-ph.HE].
[15] D.J. Reardon, et al., Search for an isotropic gravitational-wave background with the parkes pulsar timing array, Astrophys. J. Lett. 951 (1) (2023) L6, arXiv:2306.16215 [astro-ph.HE].
[16] D.J. Reardon, et al., The gravitational-wave background null hypothesis: characterizing noise in millisecond pulsar arrival times with the parkes pulsar timing array, Astrophys. J. Lett. 951 (1) (2023) L7, arXiv:2306.16229 [astro-ph.HE].
[17] A. Zic, et al., The parkes pulsar timing array third data release, arXiv:2306.16230 [astro-ph.HE].
[18] H. Xu, et al., Searching for the nano-Hertz stochastic gravitational wave background with the Chinese pulsar timing array data release I, Res. Astron. Astrophys. 23 (7) (2023) 075024, arXiv:2306.16216 [astro-ph.HE].
[19] S. Choudhury, A. Karde, S. Panda, M. Sami, Scalar induced gravity waves from ultra slow-roll Galileon inflation, arXiv:2308.09273 [astro-ph.CO].
[20] G. Bhattacharya, S. Choudhury, K. Dey, S. Ghosh, A. Karde, N.S. Mishra, Evading no-go for PBH formation and production of SIGWs using multiple sharp transitions in EFT of single field inflation, arXiv:2309.00973 [astro-ph.CO].
[21] S. Choudhury, K. Dey, A. Karde, Untangling PBH overproduction in w-SIGWs generated by pulsar timing arrays for MST-EFT of single field inflation, arXiv:2311.15065 [astro-ph.CO].
[22] G. Franciolini, A. Iovino Junior, V. Vaskonen, H. Veermae, The recent gravitational wave observation by pulsar timing arrays and primordial black holes: the importance of non-gaussianities, arXiv:2306.17149 [astro-ph.CO].
[23] K. Inomata, K. Kohri, T. Terada, The detected stochastic gravitational waves and subsolar-mass primordial black holes, arXiv:2306.17834 [astro-ph.CO].
[24] S. Wang, Z.-C. Zhao, J.-P. Li, Q.-H. Zhu, Implications of pulsar timing array data for scalar-induced gravitational waves and primordial black holes: primordial non-Gaussianity $f_{\rm NL}$ considered, arXiv:2307.00572 [astro-ph.CO].
[25] S. Balaji, G. Domènech, G. Franciolini, Scalar-induced gravitational wave interpretation of PTA data: the role of scalar fluctuation propagation speed, arXiv:2307.08552 [gr-qc].
[26] S.A. Hosseini Mansoori, F. Felegray, A. Talebian, M. Sami, PBHs and GWs from $\mathbb{T}^2$-inflation and NANOGrav 15-year data, arXiv:2307.06757 [astro-ph.CO].
[27] M.A. Gorji, M. Sasaki, T. Suyama, Extra-tensor-induced origin for the PTA signal: no primordial black hole production, arXiv:2307.13109 [astro-ph.CO].

[28] V. De Luca, A. Kehagias, A. Riotto, How well do we know the primordial black hole abundance: the crucial role of nonlinearities when approaching the horizon, Phys. Rev. D 108 (6) (2023) 063531, arXiv:2307.13633 [astro-ph.CO].

[29] S. Choudhury, Single field inflation in the light of pulsar timing array data: quintessential interpretation of blue tilted tensor spectrum through non-bunch Davies initial condition, Eur. Phys. J. C 84 (3) (2024) 278, arXiv:2307.03249 [astro-ph.CO].

[30] Z. Yi, Q. Gao, Y. Gong, Y. Wang, F. Zhang, The waveform of the scalar induced gravitational waves in light of pulsar timing array data, arXiv:2307.02467 [gr-qc].

[31] Y.-F. Cai, X.-C. He, X. Ma, S.-F. Yan, G.-W. Yuan, Limits on scalar-induced gravitational waves from the stochastic background by pulsar timing array observations, arXiv:2306.17822 [gr-qc].

[32] Y. Cai, M. Zhu, Y.-S. Piao, Primordial black holes from null energy condition violation during inflation, arXiv:2305.10933 [gr-qc].

[33] H.-L. Huang, Y. Cai, J.-Q. Jiang, J. Zhang, Y.-S. Piao, Supermassive primordial black holes in multiverse: for nano-Hertz gravitational wave and high-redshift JWST galaxies, arXiv:2306.17577 [gr-qc].

[34] S. Vagnozzi, Inflationary interpretation of the stochastic gravitational wave background signal detected by pulsar timing array experiments, J. High Energy Astrophys. 39 (2023) 81–98, arXiv:2306.16912 [astro-ph.CO].

[35] L. Frosina, A. Urbano, On the inflationary interpretation of the nHz gravitational-wave background, arXiv:2308.06915 [astro-ph.CO].

[36] Q.-H. Zhu, Z.-C. Zhao, S. Wang, Joint implications of BBN, CMB, and PTA datasets for scalar-induced gravitational waves of second and third orders, arXiv:2307.03095 [astro-ph.CO].

[37] J.-Q. Jiang, Y. Cai, G. Ye, Y.-S. Piao, Broken blue-tilted inflationary gravitational waves: a joint analysis of NANOGrav 15-year and BICEP/Keck 2018 data, arXiv:2307.15547 [astro-ph.CO].

[38] K. Cheung, C.J. Ouseph, P.-Y. Tseng, NANOGrav signal and PBH from the modified Higgs inflation, arXiv:2307.08046 [hep-ph].

[39] V.K. Oikonomou, Flat energy spectrum of primordial gravitational waves versus peaks and the NANOGrav 2023 observation, Phys. Rev. D 108 (4) (2023) 043516, arXiv:2306.17351 [astro-ph.CO].

[40] L. Liu, Z.-C. Chen, Q.-G. Huang, Probing the equation of state of the early universe with pulsar timing arrays, arXiv:2307.14911 [astro-ph.CO].

[41] L. Liu, Z.-C. Chen, Q.-G. Huang, Implications for the non-Gaussianity of curvature perturbation from pulsar timing arrays, arXiv:2307.01102 [astro-ph.CO].

[42] Z. Wang, L. Lei, H. Jiao, L. Feng, Y.-Z. Fan, The nanohertz stochastic gravitational-wave background from cosmic string loops and the abundant high redshift massive galaxies, arXiv:2306.17150 [astro-ph.HE].

[43] L. Zu, C. Zhang, Y.-Y. Li, Y.-C. Gu, Y.-L.S. Tsai, Y.-Z. Fan, Mirror QCD phase transition as the origin of the nanohertz stochastic gravitational-wave background, arXiv:2306.16769 [astro-ph.HE].

[44] K.T. Abe, Y. Tada, Translating nano-Hertz gravitational wave background into primordial perturbations taking account of the cosmological QCD phase transition, arXiv:2307.01653 [astro-ph.CO].

[45] Y. Gouttenoire, First-order phase transition interpretation of PTA signal produces solar-mass black holes, arXiv:2307.04239 [hep-ph].

[46] A. Salvio, Supercooling in radiative symmetry breaking: theory extensions, gravitational wave detection and primordial black holes, arXiv:2307.04694 [hep-ph].

[47] X. Xue, et al., Constraining cosmological phase transitions with the parkes pulsar timing array, Phys. Rev. Lett. 127 (25) (2021) 251303, arXiv:2110.03096 [astro-ph.CO].

[48] Y. Nakai, M. Suzuki, F. Takahashi, M. Yamada, Gravitational waves and dark radiation from dark phase transition: connecting NANOGrav pulsar timing data and Hubble tension, Phys. Lett. B 816 (2021) 136238, arXiv:2009.09754 [astro-ph.CO].

[49] P. Athron, A. Fowlie, C.-T. Lu, L. Morris, L. Wu, Y. Wu, Z. Xu, Can supercooled phase transitions explain the gravitational wave background observed by pulsar timing arrays?, arXiv:2306.17239 [hep-ph].

[50] I. Ben-Dayan, U. Kumar, U. Thattarampilly, A. Verma, Probing the early universe cosmology with NANOGrav: possibilities and limitations, arXiv:2307.15123 [astro-ph.CO].

[51] E. Madge, E. Morgante, C. Puchades-Ibáñez, N. Ramberg, W. Ratzinger, S. Schenk, P. Schwaller, Primordial gravitational waves in the nano-Hertz regime and PTA data – towards solving the GW inverse problem, arXiv:2306.14856 [hep-ph].

[52] N. Kitajima, J. Lee, K. Murai, F. Takahashi, W. Yin, Nanohertz gravitational waves from axion domain walls coupled to QCD, arXiv:2306.17146 [hep-ph].

[53] E. Babichev, D. Gorbunov, S. Ramazanov, R. Samanta, A. Vikman, NANOGrav spectral index $\gamma = 3$ from melting domain walls, arXiv:2307.04582 [hep-ph].

[54] Z. Zhang, C. Cai, Y.-H. Su, S. Wang, Z.-H. Yu, H.-H. Zhang, Nano-Hertz gravitational waves from collapsing domain walls associated with freeze-in dark matter in light of pulsar timing array observations, arXiv:2307.11495 [hep-ph].

[55] Z.-M. Zeng, J. Liu, Z.-K. Guo, Enhanced curvature perturbations from spherical domain walls nucleated during inflation, arXiv:2301.07230 [astro-ph.CO].

[56] R.Z. Ferreira, A. Notari, O. Pujolas, F. Rompineve, Gravitational waves from domain walls in pulsar timing array datasets, J. Cosmol. Astropart. Phys. 02 (2023) 001, arXiv:2204.04228 [astro-ph.CO].

[57] H. An, C. Yang, Gravitational waves produced by domain walls during inflation, arXiv:2304.02361 [hep-ph].

[58] X.-F. Li, Probing the high temperature symmetry breaking with gravitational waves from domain walls, arXiv:2307.03163 [hep-ph].

[59] J.J. Blanco-Pillado, K.D. Olum, J.M. Wachter, Comparison of cosmic string and superstring models to NANOGrav 12.5-year results, Phys. Rev. D 103 (10) (2021) 103512, arXiv:2102.08194 [astro-ph.CO].

[60] W. Buchmuller, V. Domcke, K. Schmitz, Stochastic gravitational-wave background from metastable cosmic strings, J. Cosmol. Astropart. Phys. 12 (12) (2021) 006, arXiv:2107.04578 [hep-ph].

[61] J. Ellis, M. Lewicki, Cosmic string interpretation of NANOGrav pulsar timing data, Phys. Rev. Lett. 126 (4) (2021) 041304, arXiv:2009.06555 [astro-ph.CO].

[62] W. Buchmuller, V. Domcke, K. Schmitz, From NANOGrav to LIGO with metastable cosmic strings, Phys. Lett. B 811 (2020) 135914, arXiv:2009.10649 [astro-ph.CO].

[63] S. Blasi, V. Brdar, K. Schmitz, Has NANOGrav found first evidence for cosmic strings?, Phys. Rev. Lett. 126 (4) (2021) 041305, arXiv:2009.06607 [astro-ph.CO].

[64] Z. Yi, Z.-Q. You, Y. Wu, Z.-C. Chen, L. Liu, Exploring the NANOGrav signal and planet-mass primordial black holes through Higgs inflation, arXiv:2308.14688 [astro-ph.CO].

[65] M.R. Gangopadhyay, V.V. Godithi, K. Ichiki, R. Inui, T. Kajino, A. Manusankar, G.J. Mathews, Yogesh, Is NanoGRAV signals pointing towards resonant particle creation during inflation?, arXiv:2309.03101 [astro-ph.CO].

[66] S. Vagnozzi, Implications of the NANOGrav results for inflation, Mon. Not. R. Astron. Soc. 502 (1) (2021) L11–L15, arXiv:2009.13432 [astro-ph.CO].

[67] M. Benetti, L.L. Graef, S. Vagnozzi, Primordial gravitational waves from NANOGrav: a broken power-law approach, Phys. Rev. D 105 (4) (2022) 043520, arXiv:2111.04758 [astro-ph.CO].

[68] K. Inomata, M. Kawasaki, K. Mukaida, T.T. Yanagida, Axion curvaton model for the gravitational waves observed by pulsar timing arrays, arXiv:2309.11398 [astro-ph.CO].

[69] K.D. Lozanov, S. Pi, M. Sasaki, V. Takhistov, A. Wang, Axion universal gravitational wave interpretation of pulsar timing array data, arXiv:2310.03594 [astro-ph.CO].

[70] S. Basilakos, D.V. Nanopoulos, T. Papanikolaou, E.N. Saridakis, C. Tzerefos, Induced gravitational waves from flipped SU(5) superstring theory at nHz, arXiv:2309.15820 [astro-ph.CO].

[71] S. Basilakos, D.V. Nanopoulos, T. Papanikolaou, E.N. Saridakis, C. Tzerefos, Gravitational wave signatures of no-scale supergravity in NANOGrav and beyond, arXiv:2307.08601 [hep-th].

[72] J.-P. Li, S. Wang, Z.-C. Zhao, K. Kohri, Complete analysis of scalar-induced gravitational waves and primordial non-gaussianities $f_{\rm NL}$ and $g_{\rm NL}$, arXiv:2309.07792 [astro-ph.CO].

[73] G. Domènech, Scalar induced gravitational waves review, Universe 7 (11) (2021) 398, arXiv:2109.01398 [gr-qc].

[74] C. Yuan, Q.-G. Huang, A topic review on probing primordial black hole dark matter with scalar induced gravitational waves, arXiv:2103.04739 [astro-ph.GA].

[75] Z.-C. Chen, C. Yuan, Q.-G. Huang, Pulsar timing array constraints on primordial black holes with NANOGrav 11-year dataset, Phys. Rev. Lett. 124 (25) (2020) 251101, arXiv:1910.12239 [astro-ph.CO].

[76] J. Cang, Y. Gao, Y. Liu, S. Sun, High frequency gravitational waves from pulsar timing arrays, arXiv:2309.15069 [astro-ph.CO].

[77] J. Cang, Y.-Z. Ma, Y. Gao, Implications for primordial black holes from cosmological constraints on scalar-induced gravitational waves, Astrophys. J. 949 (2) (2023) 64, arXiv:2210.03476 [astro-ph.CO].

[78] R.A. Konoplya, A. Zhidenko, Asymptotic tails of massive gravitons in light of pulsar timing array observations, arXiv:2307.01110 [gr-qc].

[79] S. Matarrese, O. Pantano, D. Saez, A general relativistic approach to the nonlinear evolution of collisionless matter, Phys. Rev. D 47 (1993) 1311–1323.

[80] S. Matarrese, O. Pantano, D. Saez, General relativistic dynamics of irrotational dust: cosmological implications, Phys. Rev. Lett. 72 (1994) 320–323, arXiv:astro-ph/9310036.

[81] S. Matarrese, S. Mollerach, M. Bruni, Second order perturbations of the Einstein-de Sitter universe, Phys. Rev. D 58 (1998) 043504, arXiv:astro-ph/9707278.

[82] K.N. Ananda, C. Clarkson, D. Wands, The cosmological gravitational wave background from primordial density perturbations, Phys. Rev. D 75 (2007) 123518, arXiv:gr-qc/0612013.

[83] D. Baumann, P.J. Steinhardt, K. Takahashi, K. Ichiki, Gravitational wave spectrum induced by primordial scalar perturbations, Phys. Rev. D 76 (2007) 084019, arXiv:hep-th/0703290.

[84] Y.B. Zel'dovich, I.D. Novikov, The hypothesis of cores retarded during expansion and the hot cosmological model, Sov. Astron., A.J. (Engl. Transl.) 10 (1967) 602.

[85] S.W. Hawking, Black hole explosions, Nature 248 (1974) 30–31.

[86] B.J. Carr, S.W. Hawking, Black holes in the early universe, Mon. Not. R. Astron. Soc. 168 (1974) 399–415.

[87] B.J. Carr, The primordial black hole mass spectrum, Astrophys. J. 201 (1975) 1–19.

[88] G.F. Chapline, Cosmological effects of primordial black holes, Nature 253 (5489) (1975) 251–252.

[89] B.J. Carr, J.E. Lidsey, Primordial black holes and generalized constraints on chaotic inflation, Phys. Rev. D 48 (1993) 543–553.

[90] S. Choudhury, S. Pal, Primordial non-Gaussian features from DBI Galileon inflation, Eur. Phys. J. C 75 (6) (2015) 241, arXiv:1210.4478 [hep-th].

[91] S. Choudhury, S. Pal, DBI Galileon inflation in background SUGRA, Nucl. Phys. B 874 (2013) 85–114, arXiv:1208.4433 [hep-th].

[92] S. Choudhury, A. Mazumdar, Primordial blackholes and gravitational waves for an inflection-point model of inflation, Phys. Lett. B 733 (2014) 270–275, arXiv:1307.5119 [astro-ph.CO].

[93] J. Yokoyama, Chaotic new inflation and formation of primordial black holes, Phys. Rev. D 58 (1998) 083510, arXiv:astro-ph/9802357.

[94] M. Kawasaki, T. Yanagida, Primordial black hole formation in supergravity, Phys. Rev. D 59 (1999) 043512, arXiv:hep-ph/9807544.

[95] S.G. Rubin, A.S. Sakharov, M.Y. Khlopov, The formation of primary galactic nuclei during phase transitions in the early universe, J. Exp. Theor. Phys. 91 (2001) 921–929, arXiv:hep-ph/0106187.

[96] M.Y. Khlopov, S.G. Rubin, A.S. Sakharov, Strong primordial inhomogeneities and galaxy formation, arXiv:astro-ph/0202505.

[97] M.Y. Khlopov, S.G. Rubin, A.S. Sakharov, Primordial structure of massive black hole clusters, Astropart. Phys. 23 (2005) 265, arXiv:astro-ph/0401532.

[98] R. Saito, J. Yokoyama, R. Nagata, Single-field inflation, anomalous enhancement of superhorizon fluctuations, and non-Gaussianity in primordial black hole formation, J. Cosmol. Astropart. Phys. 06 (2008) 024, arXiv:0804.3470 [astro-ph].

[99] M.Y. Khlopov, Primordial black holes, Res. Astron. Astrophys. 10 (2010) 495–528, arXiv:0801.0116 [astro-ph].

[100] B.J. Carr, K. Kohri, Y. Sendouda, J. Yokoyama, New cosmological constraints on primordial black holes, Phys. Rev. D 81 (2010) 104019, arXiv:0912.5297 [astro-ph.CO].

[101] S. Choudhury, S. Pal, Fourth level MSSM inflation from new flat directions, J. Cosmol. Astropart. Phys. 04 (2012) 018, arXiv:1111.3441 [hep-ph].

[102] D.H. Lyth, Primordial black hole formation and hybrid inflation, arXiv:1107.1681 [astro-ph.CO].

[103] M. Drees, E. Erfani, Running spectral index and formation of primordial black hole in single field inflation models, J. Cosmol. Astropart. Phys. 01 (2012) 035, arXiv:1110.6052 [astro-ph.CO].

[104] M. Drees, E. Erfani, Running-mass inflation model and primordial black holes, J. Cosmol. Astropart. Phys. 04 (2011) 005, arXiv:1102.2340 [hep-ph].

[105] J.M. Ezquiaga, J. Garcia-Bellido, E. Ruiz Morales, Primordial black hole production in critical Higgs inflation, Phys. Lett. B 776 (2018) 345–349, arXiv:1705.04861 [astro-ph.CO].

[106] K. Kannike, L. Marzola, M. Raidal, H. Veermäe, Single field double inflation and primordial black holes, J. Cosmol. Astropart. Phys. 09 (2017) 020, arXiv:1705.06225 [astro-ph.CO].

[107] M.P. Hertzberg, M. Yamada, Primordial black holes from polynomial potentials in single field inflation, Phys. Rev. D 97 (8) (2018) 083509, arXiv:1712.09750 [astro-ph.CO].

[108] S. Pi, Y.-l. Zhang, Q.-G. Huang, M. Sasaki, Scalaron from R^2-gravity as a heavy field, J. Cosmol. Astropart. Phys. 05 (2018) 042, arXiv:1712.09896 [astro-ph.CO].

[109] T.-J. Gao, Z.-K. Guo, Primordial black hole production in inflationary models of supergravity with a single chiral superfield, Phys. Rev. D 98 (6) (2018) 063526, arXiv:1806.09320 [hep-ph].

[110] I. Dalianis, A. Kehagias, G. Tringas, Primordial black holes from α-attractors, J. Cosmol. Astropart. Phys. 01 (2019) 037, arXiv:1805.09483 [astro-ph.CO].

[111] M. Cicoli, V.A. Diaz, F.G. Pedro, Primordial black holes from string inflation, J. Cosmol. Astropart. Phys. 06 (2018) 034, arXiv:1803.02837 [hep-th].

[112] O. Özsoy, S. Parameswaran, G. Tasinato, I. Zavala, Mechanisms for primordial black hole production in string theory, J. Cosmol. Astropart. Phys. 07 (2018) 005, arXiv:1803.07626 [hep-th].

[113] C.T. Byrnes, P.S. Cole, S.P. Patil, Steepest growth of the power spectrum and primordial black holes, J. Cosmol. Astropart. Phys. 06 (2019) 028, arXiv:1811.11158 [astro-ph.CO].

[114] G. Ballesteros, J. Beltran Jimenez, M. Pieroni, Black hole formation from a general quadratic action for inflationary primordial fluctuations, J. Cosmol. Astropart. Phys. 06 (2019) 016, arXiv:1811.03065 [astro-ph.CO].

[115] K.M. Belotsky, V.I. Dokuchaev, Y.N. Eroshenko, E.A. Esipova, M.Y. Khlopov, L.A. Khromykh, A.A. Kirillov, V.V. Nikulin, S.G. Rubin, I.V. Svadkovsky, Clusters of primordial black holes, Eur. Phys. J. C 79 (3) (2019) 246, arXiv:1807.06590 [astro-ph.CO].

[116] J. Martin, T. Papanikolaou, V. Vennin, Primordial black holes from the preheating instability in single-field inflation, J. Cosmol. Astropart. Phys. 01 (2020) 024, arXiv:1907.04236 [astro-ph.CO].

[117] J.M. Ezquiaga, J. García-Bellido, V. Vennin, The exponential tail of inflationary fluctuations: consequences for primordial black holes, J. Cosmol. Astropart. Phys. 03 (2020) 029, arXiv:1912.05399 [astro-ph.CO].

[118] H. Motohashi, S. Mukohyama, M. Oliosi, Constant roll and primordial black holes, J. Cosmol. Astropart. Phys. 03 (2020) 002, arXiv:1910.13235 [gr-qc].

[119] C. Fu, P. Wu, H. Yu, Primordial black holes from inflation with nonminimal derivative coupling, Phys. Rev. D 100 (6) (2019) 063532, arXiv:1907.05042 [astro-ph.CO].

[120] A. Ashoorioon, A. Rostami, J.T. Firouzjaee, EFT compatible PBHs: effective spawning of the seeds for primordial black holes during inflation, J. High Energy Phys. 07 (2021) 087, arXiv:1912.13326 [astro-ph.CO].

[121] P. Auclair, V. Vennin, Primordial black holes from metric preheating: mass fraction in the excursion-set approach, J. Cosmol. Astropart. Phys. 02 (2021) 038, arXiv:2011.05633 [astro-ph.CO].

[122] V. Vennin, Stochastic inflation and primordial black holes, PhD thesis, U. Paris-Saclay, 6, arXiv:2009.08715 [astro-ph.CO], 2020.

[123] D.V. Nanopoulos, V.C. Spanos, I.D. Stamou, Primordial black holes from no-scale supergravity, Phys. Rev. D 102 (8) (2020) 083536, arXiv:2008.01457 [astro-ph.CO].

[124] K. Inomata, E. McDonough, W. Hu, Primordial black holes arise when the inflaton falls, Phys. Rev. D 104 (12) (2021) 123553, arXiv:2104.03972 [astro-ph.CO].

[125] I.D. Stamou, Mechanisms of producing primordial black holes by breaking the $SU(2,1)/SU(2)\times U(1)$ symmetry, Phys. Rev. D 103 (8) (2021) 083512, arXiv:2104.08654 [hep-ph].

[126] K.-W. Ng, Y.-P. Wu, Constant-rate inflation: primordial black holes from conformal weight transitions, J. High Energy Phys. 11 (2021) 076, arXiv:2102.05620 [astro-ph.CO].

[127] Q. Wang, Y.-C. Liu, B.-Y. Su, N. Li, Primordial black holes from the perturbations in the inflaton potential in peak theory, Phys. Rev. D 104 (8) (2021) 083546, arXiv:2111.10028 [astro-ph.CO].

[128] S. Kawai, J. Kim, Primordial black holes from Gauss-Bonnet-corrected single field inflation, Phys. Rev. D 104 (8) (2021) 083545, arXiv:2108.01340 [astro-ph.CO].

[129] M. Solbi, K. Karami, Primordial black holes formation in the inflationary model with field-dependent kinetic term for quartic and natural potentials, Eur. Phys. J. C 81 (10) (2021) 884, arXiv:2106.02863 [astro-ph.CO].

[130] G. Ballesteros, S. Céspedes, L. Santoni, Large power spectrum and primordial black holes in the effective theory of inflation, J. High Energy Phys. 01 (2022) 074, arXiv:2109.00567 [hep-th].

[131] G. Rigopoulos, A. Wilkins, Inflation is always semi-classical: diffusion domination overproduces primordial black holes, J. Cosmol. Astropart. Phys. 12 (12) (2021) 027, arXiv:2107.05317 [astro-ph.CO].

[132] C. Animali, V. Vennin, Primordial black holes from stochastic tunnelling, arXiv:2210.03812 [astro-ph.CO].

[133] M. Correa, M.R. Gangopadhyay, N. Jaman, G.J. Mathews, Primordial black-hole dark matter via warm natural inflation, Phys. Lett. B 835 (2022) 137510, arXiv:2207.10394 [gr-qc].

[134] D. Frolovsky, S.V. Ketov, S. Saburov, Formation of primordial black holes after Starobinsky inflation, Mod. Phys. Lett. A 37 (21) (2022) 2250135, arXiv:2205.00603 [astro-ph.CO].

[135] A. Escrivà, F. Kuhnel, Y. Tada, Primordial black holes, arXiv:2211.05767 [astro-ph.CO].

[136] O. Özsoy, G. Tasinato, Inflation and primordial black holes, arXiv:2301.03600 [astro-ph.CO].

[137] P. Ivanov, P. Naselsky, I. Novikov, Inflation and primordial black holes as dark matter, Phys. Rev. D 50 (1994) 7173–7178.

[138] N. Afshordi, P. McDonald, D.N. Spergel, Primordial black holes as dark matter: the power spectrum and evaporation of early structures, Astrophys. J. Lett. 594 (2003) L71–L74, arXiv:astro-ph/0302035.

[139] P.H. Frampton, M. Kawasaki, F. Takahashi, T.T. Yanagida, Primordial black holes as all dark matter, J. Cosmol. Astropart. Phys. 04 (2010) 023, arXiv:1001.2308 [hep-ph].

[140] B. Carr, F. Kuhnel, M. Sandstad, Primordial black holes as dark matter, Phys. Rev. D 94 (8) (2016) 083504, arXiv:1607.06077 [astro-ph.CO].

[141] M. Kawasaki, A. Kusenko, Y. Tada, T.T. Yanagida, Primordial black holes as dark matter in supergravity inflation models, Phys. Rev. D 94 (8) (2016) 083523, arXiv:1606.07631 [astro-ph.CO].

[142] K. Inomata, M. Kawasaki, K. Mukaida, Y. Tada, T.T. Yanagida, Inflationary primordial black holes as all dark matter, Phys. Rev. D 96 (4) (2017) 043504, arXiv:1701.02544 [astro-ph.CO].

[143] J.R. Espinosa, D. Racco, A. Riotto, Cosmological signature of the standard model Higgs vacuum instability: primordial black holes as dark matter, Phys. Rev. Lett. 120 (12) (2018) 121301, arXiv:1710.11196 [hep-ph].

[144] G. Ballesteros, M. Taoso, Primordial black hole dark matter from single field inflation, Phys. Rev. D 97 (2) (2018) 023501, arXiv:1709.05565 [hep-ph].

[145] M. Sasaki, T. Suyama, T. Tanaka, S. Yokoyama, Primordial black holes—perspectives in gravitational wave astronomy, Class. Quantum Gravity 35 (6) (2018) 063001, arXiv:1801.05235 [astro-ph.CO].

[146] G. Ballesteros, J. Rey, F. Rompineve, Detuning primordial black hole dark matter with early matter domination and axion monodromy, J. Cosmol. Astropart. Phys. 06 (2020) 014, arXiv:1912.01638 [astro-ph.CO].

[147] I. Dalianis, G. Tringas, Primordial black hole remnants as dark matter produced in thermal, matter, and runaway-quintessence postinflationary scenarios, Phys. Rev. D 100 (8) (2019) 083512, arXiv:1905.01741 [astro-ph.CO].

[148] D.Y. Cheong, S.M. Lee, S.C. Park, Primordial black holes in Higgs-R^2 inflation as the whole of dark matter, J. Cosmol. Astropart. Phys. 01 (2021) 032, arXiv:1912.12032 [hep-ph].

[149] A.M. Green, B.J. Kavanagh, Primordial black holes as a dark matter candidate, J. Phys. G 48 (4) (2021) 043001, arXiv:2007.10722 [astro-ph.CO].

[150] B. Carr, F. Kuhnel, Primordial black holes as dark matter: recent developments, Annu. Rev. Nucl. Part. Sci. 70 (2020) 355–394, arXiv:2006.02838 [astro-ph.CO].

[151] G. Ballesteros, J. Rey, M. Taoso, A. Urbano, Primordial black holes as dark matter and gravitational waves from single-field polynomial inflation, J. Cosmol. Astropart. Phys. 07 (2020) 025, arXiv:2001.08220 [astro-ph.CO].

[152] B. Carr, K. Kohri, Y. Sendouda, J. Yokoyama, Constraints on primordial black holes, Rep. Prog. Phys. 84 (11) (2021) 116902, arXiv:2002.12778 [astro-ph.CO].

[153] O. Özsoy, Z. Lalak, Primordial black holes as dark matter and gravitational waves from bumpy axion inflation, J. Cosmol. Astropart. Phys. 01 (2021) 040, arXiv:2008.07549 [astro-ph.CO].

[154] R. Saito, J. Yokoyama, Gravitational wave background as a probe of the primordial black hole abundance, Phys. Rev. Lett. 102 (2009) 161101, arXiv:0812.4339 [astro-ph], Erratum: Phys. Rev. Lett. 107 (2011) 069901.
[155] R. Saito, J. Yokoyama, Gravitational-wave constraints on the abundance of primordial black holes, Prog. Theor. Phys. 123 (2010) 867–886, arXiv:0912.5317 [astro-ph.CO], Erratum: Prog. Theor. Phys. 126 (2011) 351–352.
[156] M. Sasaki, T. Suyama, T. Tanaka, S. Yokoyama, Primordial black hole scenario for the gravitational-wave event GW150914, Phys. Rev. Lett. 117 (6) (2016) 061101, arXiv:1603.08338 [astro-ph.CO], Erratum: Phys. Rev. Lett. 121 (2018) 059901.
[157] M. Raidal, V. Vaskonen, H. Veermäe, Gravitational waves from primordial black hole mergers, J. Cosmol. Astropart. Phys. 09 (2017) 037, arXiv:1707.01480 [astro-ph.CO].
[158] T. Papanikolaou, V. Vennin, D. Langlois, Gravitational waves from a universe filled with primordial black holes, J. Cosmol. Astropart. Phys. 03 (2021) 053, arXiv:2010.11573 [astro-ph.CO].
[159] Y. Ali-Haïmoud, E.D. Kovetz, M. Kamionkowski, Merger rate of primordial black-hole binaries, Phys. Rev. D 96 (12) (2017) 123523, arXiv:1709.06576 [astro-ph.CO].
[160] H. Di, Y. Gong, Primordial black holes and second order gravitational waves from ultra-slow-roll inflation, J. Cosmol. Astropart. Phys. 07 (2018) 007, arXiv:1707.09578 [astro-ph.CO].
[161] M. Raidal, C. Spethmann, V. Vaskonen, H. Veermäe, Formation and evolution of primordial black hole binaries in the early universe, J. Cosmol. Astropart. Phys. 02 (2019) 018, arXiv:1812.01930 [astro-ph.CO].
[162] S.-L. Cheng, W. Lee, K.-W. Ng, Primordial black holes and associated gravitational waves in axion monodromy inflation, J. Cosmol. Astropart. Phys. 07 (2018) 001, arXiv:1801.09050 [astro-ph.CO].
[163] V. Vaskonen, H. Veermäe, Lower bound on the primordial black hole merger rate, Phys. Rev. D 101 (4) (2020) 043015, arXiv:1908.09752 [astro-ph.CO].
[164] M. Drees, Y. Xu, Overshooting, critical Higgs inflation and second order gravitational wave signatures, Eur. Phys. J. C 81 (2) (2021) 182, arXiv:1905.13581 [hep-ph].
[165] A. Hall, A.D. Gow, C.T. Byrnes, Bayesian analysis of LIGO-Virgo mergers: primordial vs. astrophysical black hole populations, Phys. Rev. D 102 (2020) 123524, arXiv:2008.13704 [astro-ph.CO].
[166] A. Ashoorioon, A. Rostami, J.T. Firouzjaee, Examining the end of inflation with primordial black holes mass distribution and gravitational waves, Phys. Rev. D 103 (2021) 123512, arXiv:2012.02817 [astro-ph.CO].
[167] L. Wu, Y. Gong, T. Li, Primordial black holes and secondary gravitational waves from string inspired general no-scale supergravity, Phys. Rev. D 104 (12) (2021) 123544, arXiv:2105.07694 [gr-qc].
[168] R. Kimura, T. Suyama, M. Yamaguchi, Y.-L. Zhang, Reconstruction of primordial power spectrum of curvature perturbation from the merger rate of primordial black hole binaries, J. Cosmol. Astropart. Phys. 04 (2021) 031, arXiv:2102.05280 [astro-ph.CO].
[169] M. Solbi, K. Karami, Primordial black holes and induced gravitational waves in k-inflation, J. Cosmol. Astropart. Phys. 08 (2021) 056, arXiv:2102.05651 [astro-ph.CO].
[170] Z. Teimoori, K. Rezazadeh, M.A. Rasheed, K. Karami, Mechanism of primordial black holes production and secondary gravitational waves in α-attractor Galileon inflationary scenario, arXiv:2107.07620 [astro-ph.CO].
[171] M. Cicoli, F.G. Pedro, N. Pedron, Secondary GWs and PBHs in string inflation: formation and detectability, J. Cosmol. Astropart. Phys. 08 (08) (2022) 030, arXiv:2203.00021 [hep-th].
[172] A. Ashoorioon, K. Rezazadeh, A. Rostami, NANOGrav signal from the end of inflation and the LIGO mass and heavier primordial black holes, Phys. Lett. B 835 (2022) 137542, arXiv:2202.01131 [astro-ph.CO].
[173] T. Papanikolaou, Gravitational waves induced from primordial black hole fluctuations: the effect of an extended mass function, J. Cosmol. Astropart. Phys. 10 (2022) 089, arXiv:2207.11041 [astro-ph.CO].
[174] T. Papanikolaou, Primordial black holes in loop quantum cosmology: the effect on the threshold, Class. Quantum Gravity 40 (13) (2023) 134001, arXiv:2301.11439 [gr-qc].
[175] X. Wang, Y.-l. Zhang, R. Kimura, M. Yamaguchi, Reconstruction of power spectrum of primordial curvature perturbations on small scales from primordial black hole binaries scenario of LIGO/VIRGO detection, arXiv:2209.12911 [astro-ph.CO].
[176] R. Zheng, J. Shi, T. Qiu, On primordial black holes and secondary gravitational waves generated from inflation with solo/multi-bumpy potential, Chin. Phys. C 46 (4) (2022) 045103, arXiv:2106.04303 [astro-ph.CO].
[177] T. Cohen, D. Green, A. Premkumar, Large deviations in the early universe, arXiv:2212.02535 [hep-th].
[178] R. Arya, Formation of primordial black holes from warm inflation, J. Cosmol. Astropart. Phys. 09 (2020) 042, arXiv:1910.05238 [astro-ph.CO].
[179] A.R. Brown, Hyperbolic inflation, Phys. Rev. Lett. 121 (25) (2018) 251601, arXiv:1705.03023 [hep-th].
[180] G.A. Palma, S. Sypsas, C. Zenteno, Seeding primordial black holes in multifield inflation, Phys. Rev. Lett. 125 (12) (2020) 121301, arXiv:2004.06106 [astro-ph.CO].
[181] S.R. Geller, W. Qin, E. McDonough, D.I. Kaiser, Primordial black holes from multifield inflation with nonminimal couplings, Phys. Rev. D 106 (6) (2022) 063535, arXiv:2205.04471 [hep-th].
[182] M. Braglia, A. Linde, R. Kallosh, F. Finelli, Hybrid α-attractors, primordial black holes and gravitational wave backgrounds, arXiv:2211.14262 [astro-ph.CO].
[183] D. Frolovsky, S.V. Ketov, Fitting power spectrum of scalar perturbations for primordial black hole production during inflation, arXiv:2302.06153 [astro-ph.CO].
[184] Y. Aldabergenov, S.V. Ketov, Primordial black holes from Volkov-Akulov-Starobinsky supergravity, arXiv:2301.12750 [hep-th].
[185] S. Aoki, R. Ishikawa, S.V. Ketov, Pole inflation and primordial black holes formation in Starobinsky-like supergravity, Class. Quantum Gravity 40 (6) (2023) 065002, arXiv:2210.10348 [hep-th].
[186] D. Frolovsky, S.V. Ketov, S. Saburov, E-models of inflation and primordial black holes, Front. Phys. 10 (2022) 1005333, arXiv:2207.11878 [astro-ph.CO].
[187] Y. Aldabergenov, A. Addazi, S.V. Ketov, Inflation, SUSY breaking, and primordial black holes in modified supergravity coupled to chiral matter, Eur. Phys. J. C 82 (8) (2022) 681, arXiv:2206.02601 [astro-ph.CO].
[188] R. Ishikawa, S.V. Ketov, Exploring the parameter space of modified supergravity for double inflation and primordial black hole formation, Class. Quantum Gravity 39 (1) (2022) 015016, arXiv:2108.04408 [astro-ph.CO].
[189] A. Gundhi, S.V. Ketov, C.F. Steinwachs, Primordial black hole dark matter in dilaton-extended two-field Starobinsky inflation, Phys. Rev. D 103 (8) (2021) 083518, arXiv:2011.05999 [hep-th].
[190] Y. Aldabergenov, A. Addazi, S.V. Ketov, Primordial black holes from modified supergravity, Eur. Phys. J. C 80 (10) (2020) 917, arXiv:2006.16641 [hep-th].
[191] R.-g. Cai, S. Pi, M. Sasaki, Gravitational waves induced by non-Gaussian scalar perturbations, Phys. Rev. Lett. 122 (20) (2019) 201101, arXiv:1810.11000 [astro-ph.CO].
[192] S.-L. Cheng, D.-S. Lee, K.-W. Ng, Power spectrum of primordial perturbations during ultra-slow-roll inflation with back reaction effects, Phys. Lett. B 827 (2022) 136956, arXiv:2106.09275 [astro-ph.CO].
[193] S. Balaji, J. Silk, Y.-P. Wu, Induced gravitational waves from the cosmic coincidence, J. Cosmol. Astropart. Phys. 06 (06) (2022) 008, arXiv:2202.00700 [astro-ph.CO].
[194] W. Qin, S.R. Geller, S. Balaji, E. McDonough, D.I. Kaiser, Planck constraints and gravitational wave forecasts for primordial black hole dark matter seeded by multifield inflation, arXiv:2303.02168 [astro-ph.CO].
[195] A. Riotto, The primordial black hole formation from single-field inflation is not ruled out, arXiv:2301.00599 [astro-ph.CO].
[196] H.V. Ragavendra, L. Sriramkumar, J. Silk, Could PBHs and secondary GWs have originated from squeezed initial states?, J. Cosmol. Astropart. Phys. 05 (2021) 010, arXiv:2011.09938 [astro-ph.CO].
[197] H.V. Ragavendra, Accounting for scalar non-Gaussianity in secondary gravitational waves, Phys. Rev. D 105 (6) (2022) 063533, arXiv:2108.04193 [astro-ph.CO].
[198] H.V. Ragavendra, P. Saha, L. Sriramkumar, J. Silk, Primordial black holes and secondary gravitational waves from ultraslow roll and punctuated inflation, Phys. Rev. D 103 (8) (2021) 083510, arXiv:2008.12202 [astro-ph.CO].
[199] M.R. Gangopadhyay, J.C. Jain, D. Sharma, Yogesh, Production of primordial black holes via single field inflation and observational constraints, Eur. Phys. J. C 82 (9) (2022) 849, arXiv:2108.13839 [astro-ph.CO].
[200] T. Papanikolaou, A. Lymperis, S. Lola, E.N. Saridakis, Primordial black holes and gravitational waves from non-canonical inflation, J. Cosmol. Astropart. Phys. 03 (2023) 003, arXiv:2211.14900 [astro-ph.CO].
[201] S. Choudhury, A. Karde, P. Padiyar, M. Sami, Primordial black holes from effective field theory of stochastic single field inflation at NNNLO, arXiv:2403.13484 [astro-ph.CO].
[202] S. Choudhury, A. Karde, S. Panda, S. SenGupta, Regularized-renormalized-resummed loop corrected power spectrum of non-singular bounce with primordial black hole formation, arXiv:2405.06882 [astro-ph.CO].
[203] S. Choudhury, Large fluctuations in the Sky, arXiv:2403.07343 [astro-ph.CO].
[204] S. Choudhury, M. Sami, Large fluctuations and primordial black holes, arXiv:2407.17006 [gr-qc].
[205] G. Ferrante, G. Franciolini, A. Iovino Junior, A. Urbano, Primordial non-Gaussianity up to all orders: theoretical aspects and implications for primordial black hole models, Phys. Rev. D 107 (4) (2023) 043520, arXiv:2211.01728 [astro-ph.CO].
[206] M.A. Gorji, M. Sasaki, Primordial-tensor-induced stochastic gravitational waves, arXiv:2302.14080 [gr-qc].
[207] J. Kristiano, J. Yokoyama, Ruling out primordial black hole formation from single-field inflation, arXiv:2211.03395 [hep-th].
[208] S. Banerjee, S. Choudhury, S. Chowdhury, J. Knaute, S. Panda, K. Shirish, Thermalization in quenched open quantum cosmology, Nucl. Phys. B 996 (2023) 116368, arXiv:2104.10692 [hep-th].
[209] S. Choudhury, M.R. Gangopadhyay, M. Sami, No-go for the formation of heavy mass primordial black holes in single field inflation, arXiv:2301.10000 [astro-ph.CO].
[210] S. Choudhury, S. Panda, M. Sami, PBH formation in EFT of single field inflation with sharp transition, Phys. Lett. B 845 (2023) 138123, arXiv:2302.05655 [astro-ph.CO].
[211] S. Choudhury, S. Panda, M. Sami, Quantum loop effects on the power spectrum and constraints on primordial black holes, arXiv:2303.06066 [astro-ph.CO].
[212] S. Choudhury, S. Panda, M. Sami, Galileon inflation evades the no-go for PBH formation in the single-field framework, J. Cosmol. Astropart. Phys. 08 (2023) 078, arXiv:2304.04065 [astro-ph.CO].
[213] S. Choudhury, A. Karde, S. Panda, M. Sami, Primordial non-Gaussianity from ultra slow-roll Galileon inflation, arXiv:2306.12334 [astro-ph.CO].

[214] J. Kristiano, J. Yokoyama, Response to criticism on "Ruling out primordial black hole formation from single-field inflation": a note on bispectrum and one-loop correction in single-field inflation with primordial black hole formation, arXiv:2303.00341 [hep-th].
[215] A. Riotto, The primordial black hole formation from single-field inflation is still not ruled out, arXiv:2303.01727 [astro-ph.CO].
[216] H. Firouzjahi, A. Riotto, Primordial black holes and loops in single-field inflation, arXiv:2304.07801 [astro-ph.CO].
[217] H. Firouzjahi, One-loop corrections in power spectrum in single field inflation, arXiv:2303.12025 [astro-ph.CO].
[218] G. Franciolini, A. Iovino Junior, M. Taoso, A. Urbano, One loop to rule them all: perturbativity in the presence of ultra slow-roll dynamics, arXiv:2305.03491 [astro-ph.CO].
[219] S.-L. Cheng, D.-S. Lee, K.-W. Ng, Primordial perturbations from ultra-slow-roll single-field inflation with quantum loop effects, arXiv:2305.16810 [astro-ph.CO].
[220] G. Tasinato, A large $|\eta|$ approach to single field inflation, arXiv:2305.11568 [hep-th].
[221] H. Motohashi, Y. Tada, Squeezed bispectrum and one-loop corrections in transient constant-roll inflation, arXiv:2303.16035 [astro-ph.CO].
[222] G. Ferrante, G. Franciolini, A. Iovino Junior, A. Urbano, Primordial black holes in the curvaton model: possible connections to pulsar timing arrays and dark matter, J. Cosmol. Astropart. Phys. 06 (2023) 057, arXiv:2305.13382 [astro-ph.CO].
[223] A.D. Gow, T. Miranda, S. Nurmi, Primordial black holes from a curvaton scenario with strongly non-Gaussian perturbations, arXiv:2307.03078 [astro-ph.CO].
[224] H. Firouzjahi, A. Riotto, The sign of non-Gaussianity and the primordial black holes abundance, arXiv:2309.10536 [astro-ph.CO].
[225] LISA Collaboration, P. Amaro-Seoane, et al., Laser interferometer space antenna, arXiv:1702.00786 [astro-ph.IM].
[226] S. Kawamura, et al., The Japanese space gravitational wave antenna: DECIGO, Class. Quantum Gravity 28 (2011) 094011.
[227] M. Punturo, et al., The Einstein telescope: a third-generation gravitational wave observatory, Class. Quantum Gravity 27 (2010) 194002.
[228] D. Reitze, et al., Cosmic explorer: the U.S. contribution to gravitational-wave astronomy beyond LIGO, Bull. Am. Astron. Soc. 51 (7) (2019) 035, arXiv:1907.04833 [astro-ph.IM].
[229] J. Crowder, N.J. Cornish, Beyond LISA: exploring future gravitational wave missions, Phys. Rev. D 72 (2005) 083005, arXiv:gr-qc/0506015.
[230] LIGO Scientific Collaboration, J. Aasi, et al., Advanced LIGO, Class. Quantum Gravity 32 (2015) 074001, arXiv:1411.4547 [gr-qc].
[231] VIRGO Collaboration, F. Acernese, et al., Advanced Virgo: a second-generation interferometric gravitational wave detector, Class. Quantum Gravity 32 (2) (2015) 024001, arXiv:1408.3978 [gr-qc].
[232] KAGRA Collaboration, T. Akutsu, et al., KAGRA: 2.5 generation interferometric gravitational wave detector, Nat. Astron. 3 (1) (2019) 35–40, arXiv:1811.08079 [gr-qc].
[233] I. Musco, V. De Luca, G. Franciolini, A. Riotto, Threshold for primordial black holes. II. A simple analytic prescription, Phys. Rev. D 103 (6) (2021) 063538, arXiv:2011.03014 [astro-ph.CO].
[234] A. Kehagias, I. Musco, A. Riotto, Non-Gaussian formation of primordial black holes: effects on the threshold, J. Cosmol. Astropart. Phys. 12 (2019) 029, arXiv:1906.07135 [astro-ph.CO].
[235] S. Young, I. Musco, C.T. Byrnes, Primordial black hole formation and abundance: contribution from the non-linear relation between the density and curvature perturbation, J. Cosmol. Astropart. Phys. 11 (2019) 012, arXiv:1904.00984 [astro-ph.CO].
[236] I. Musco, Threshold for primordial black holes: dependence on the shape of the cosmological perturbations, Phys. Rev. D 100 (12) (2019) 123524, arXiv:1809.02127 [gr-qc].
[237] A.D. Gow, H. Assadullahi, J.H.P. Jackson, K. Koyama, V. Vennin, D. Wands, Non-perturbative non-Gaussianity and primordial black holes, Europhys. Lett. 142 (4) (2023) 49001, arXiv:2211.08348 [astro-ph.CO].
[238] M. Biagetti, V. De Luca, G. Franciolini, A. Kehagias, A. Riotto, The formation probability of primordial black holes, Phys. Lett. B 820 (2021) 136602, arXiv:2105.07810 [astro-ph.CO].
[239] C. Burrage, C. de Rham, D. Seery, A.J. Tolley, Galileon inflation, J. Cosmol. Astropart. Phys. 01 (2011) 014, arXiv:1009.2497 [hep-th].
[240] S. Choudhury, A. Karde, S. Panda, M. Sami, Realisation of the ultra-slow roll phase in Galileon inflation and PBH overproduction, J. Cosmol. Astropart. Phys. 07 (2024) 034, arXiv:2401.10925 [astro-ph.CO].
[241] G. Goon, K. Hinterbichler, A. Joyce, M. Trodden, Aspects of Galileon non-renormalization, J. High Energy Phys. 11 (2016) 100, arXiv:1606.02295 [hep-th].
[242] K. Kohri, T. Terada, Semianalytic calculation of gravitational wave spectrum nonlinearly induced from primordial curvature perturbations, Phys. Rev. D 97 (12) (2018) 123532, arXiv:1804.08577 [gr-qc].
[243] A.G. Polnarev, I. Musco, Curvature profiles as initial conditions for primordial black hole formation, Class. Quantum Gravity 24 (2007) 1405–1432, arXiv:gr-qc/0605122.
[244] V. De Luca, A. Riotto, A note on the abundance of primordial black holes: use and misuse of the metric curvature perturbation, Phys. Lett. B 828 (2022) 137035, arXiv:2201.09008 [astro-ph.CO].
[245] M. Taoso, A. Urbano, Non-gaussianities for primordial black hole formation, J. Cosmol. Astropart. Phys. 08 (2021) 016, arXiv:2102.03610 [astro-ph.CO].
[246] V. Atal, C. Germani, The role of non-gaussianities in primordial black hole formation, Phys. Dark Universe 24 (2019) 100275, arXiv:1811.07857 [astro-ph.CO].
[247] S. Young, C.T. Byrnes, Primordial black holes in non-Gaussian regimes, J. Cosmol. Astropart. Phys. 08 (2013) 052, arXiv:1307.4995 [astro-ph.CO].
[248] C.T. Byrnes, E.J. Copeland, A.M. Green, Primordial black holes as a tool for constraining non-Gaussianity, Phys. Rev. D 86 (2012) 043512, arXiv:1206.4188 [astro-ph.CO].
[249] J.S. Bullock, J.R. Primack, NonGaussian fluctuations and primordial black holes from inflation, Phys. Rev. D 55 (1997) 7423–7439, arXiv:astro-ph/9611106.
[250] M.W. Choptuik, Universality and scaling in gravitational collapse of a massless scalar field, Phys. Rev. Lett. 70 (1993) 9–12.
[251] C.R. Evans, J.S. Coleman, Observation of critical phenomena and selfsimilarity in the gravitational collapse of radiation fluid, Phys. Rev. Lett. 72 (1994) 1782–1785, arXiv:gr-qc/9402041.
[252] S. Young, Peaks and primordial black holes: the effect of non-Gaussianity, J. Cosmol. Astropart. Phys. 05 (05) (2022) 037, arXiv:2201.13345 [astro-ph.CO].
[253] M. Shibata, M. Sasaki, Black hole formation in the Friedmann universe: formulation and computation in numerical relativity, Phys. Rev. D 60 (1999) 084002, arXiv:gr-qc/9905064.
[254] T. Harada, C.-M. Yoo, T. Nakama, Y. Koga, Cosmological long-wavelength solutions and primordial black hole formation, Phys. Rev. D 91 (8) (2015) 084057, arXiv:1503.03934 [gr-qc].
[255] V. De Luca, G. Franciolini, A. Kehagias, M. Peloso, A. Riotto, C. Ünal, The ineludible non-Gaussianity of the primordial black hole abundance, J. Cosmol. Astropart. Phys. 07 (2019) 048, arXiv:1904.00970 [astro-ph.CO].
[256] A. Escrivà, Y. Tada, S. Yokoyama, C.-M. Yoo, Simulation of primordial black holes with large negative non-Gaussianity, J. Cosmol. Astropart. Phys. 05 (05) (2022) 012, arXiv:2202.01028 [astro-ph.CO].
[257] Planck Collaboration, P.A.R. Ade, et al., Planck 2015 results. XX. Constraints on inflation, Astron. Astrophys. 594 (2016) A20, arXiv:1502.02114 [astro-ph.CO].